Quaternary Science Reviews 268 (2021) 107126

Contents lists available at ScienceDirect

Quaternary Science Reviews

journal homepage: www.elsevier.com/locate/quascirev

Invited paper

Regional shifts in paleohurricane activity over the last 1500 years derived from blue hole sediments offshore of Middle Caicos Island

Elizabeth Wallace [a, *], Jeffrey Donnelly [b], Peter van Hengstum [c, d], Tyler Winkler [d], Charmille Dizon [e], Alexandra LaBella [e], Isabella Lopez [e], Nicole d'Entremont [b], Richard Sullivan [d], Jonathan Woodruff [f], Andrea Hawkes [g], Christopher Maio [h]

[a] Massachusetts Institute of Technology/Woods Hole Oceanographic Institution Joint Program in Oceanography, Woods Hole, MA, 02543, USA
[b] Department of Geology and Geophysics, Woods Hole Oceanographic Institution, Woods Hole, MA, 02543, USA
[c] Department of Marine Sciences, Texas A&M University at Galveston, Galveston, TX, 77554, USA
[d] Department of Oceanography, Texas A&M University, College Station, TX, 77840, USA
[e] Department of Marine & Environmental Sciences, Northeastern University, Boston, MA, 02115, USA
[f] Department of Geosciences, University of Massachusetts Amherst, Amherst, MA, 01003, USA
[g] Department of Earth and Ocean Sciences, Center for Marine Science, University of North Carolina Wilmington, Wilmington, NC, 28403-5944, USA
[h] Department of Geosciences, University of Alaska Fairbanks, Fairbanks, AK, 99775, USA

ARTICLE INFO

Article history:
Received 15 April 2021
Received in revised form
26 July 2021
Accepted 27 July 2021
Available online 13 August 2021

Handling Editor: Dr A. Voelker

Keywords:
Tropical cyclones
Bahamas
Blue holes
Carbonate sediments
Paleotempestology

ABSTRACT

Coastal communities are vulnerable to sea-level rise and hurricane-induced flooding. Our ability to assess flooding risk at coastal locations is restricted by the short observational record and limited knowledge on storm surge generation during hurricanes of different strength, size and orientation. Here, we present a transect of sediment cores collected from a blue hole near Middle Caicos in the Turks & Caicos Islands. Storm deposits found across cores in the transect record the passage of hurricanes passing to the south of Middle Caicos over the past 1500 years including Hurricane Irma in 2017. The record indicates historically unprecedented multi-decadal periods of elevated storm strikes on the island. We add this new reconstruction to a compilation of near-annually resolved paleohurricane records of the past millennium in The Bahamas. This compilation indicates increased storm activity in The Bahamas from 650 to 800 CE, 930 to 1040 CE, and 1400 to 1800 CE. Taken together with compilations of published paleohurricane records from New England and the Gulf Coast of Florida, we observe periods of elevated hurricane activity in all three spatially disparate regions over the past millennium and periods when New England and the Bahama Archipelago are active while the Gulf Coast of Florida is not. We argue that both regional-scale changes in vertical wind shear patterns and shifting storm tracks may explain the discrepancies we observe between different regions of the North Atlantic. This research informs how hurricane frequency has changed over the past 1500 years specifically in the Turks & Caicos Islands and regionally along the Bahama Archipelago.

1. Introduction

Each year, tropical cyclones (TCs) form in the tropical North Atlantic Ocean moving through the Caribbean Sea, Gulf of Mexico, and/or along the U.S. eastern seaboard. As these storms approach land, they induce strong winds, storm surge and heavy rain which cause massive economic and human losses in coastal communities (Dinan et al., 2016). These losses are expected to increase in the next century with projected increases in TC intensity, rising sea levels and growing coastal populations (Knutson et al., 2020). Providing coastal communities with longer term information and context on the scale and probability of TC events is important for local planning as well as the sustainable economic development of these areas.

Unfortunately, there is still significant uncertainty on how North Atlantic TC properties (e.g., frequency, intensity, speed, tracks) will change both on a basin-scale and a regional-scale. The current set of TC observations suffers from data quality issues (Landsea et al., 2004, 2010, 2010; Vecchi and Knutson, 2008, 2011, 2011; Villarini

* Corresponding author.
E-mail address: ejwallac@rice.edu (E. Wallace).

https://doi.org/10.1016/j.quascirev.2021.107126
0277-3791/

et al., 2011; Landsea and Franklin, 2013) and only extends back over the past 169 years (1851–2020 CE). This short observational record does not allow for elucidating hurricane-climate interactions on long timescales or during climatic regimes that differ from the modern.

TC properties are related to large-scale ambient environmental conditions in the Atlantic. In particular, sea surface temperatures (SSTs) and vertical wind shear (VWS) strongly influence hurricane potential intensity (Emanuel 1987, 1988) and genesis (Camargo et al., 2007; Emanuel, 1989), respectively. Warmer SSTs provide energy to TCs in the form of moist enthalpy and TCs only develop over ocean water with surface temperature exceeding 26°C (Emanuel, 2003; Gray, 1998). Lower vertical wind shear, defined as the difference between horizontal winds in the upper (200 hPa) and lower (850 hPa) troposphere, favors hurricane convective organization and intensification (Merrill, 1987; Rios-Berrios and Torn, 2017).

There are a variety of different regional and remote climate oscillations and external forcing factors that influence changes in atmospheric steering currents, SST, and VWS patterns in the Atlantic. These include the North Atlantic Oscillation (Elsner and Kocher, 2000; Kossin et al., 2010), Atlantic Multidecadal Variability (Goldenberg et al., 2001; Clement et al., 2015; Ting et al., 2019), El Niño Southern Oscillation (ENSO) (Gray, 1984; Goldenberg and Shapiro, 1996; Chu, 2004), and volcanic eruptions (Evan, 2012; Korty et al., 2012; Pausata and Camargo, 2019), among others. Many of these mechanisms have multivariate, multi-scalar, and non-linear responses and occur on different timescales. This makes it very difficult to fully characterize the response of TC activity to these phenomena, especially over the short observational record.

There is a growing number of paleohurricane reconstructions from geologic archives that extend observations of landfalling hurricanes back thousands of years along the North American coastline (e.g., Boldt et al., 2010; Lane et al., 2011; Mallinson et al., 2011; Donnelly et al., 2015; van Hengstum et al., 2016; Bregy et al., 2018). Recent studies have obtained Common Era paleohurricane records from sediment cores in blue holes scattered across the hurricane-prone tropics (e.g., Denommee et al., 2014; van Hengstum et al., 2014; Wallace et al., 2019; Bramante et al., 2020; Schmitt et al., 2020; Winkler et al., 2020). Blue holes serve as giant traps for sediment from surrounding reefs and lagoons suspended and transported during storm events (Shinn et al., 1996).

Recent reconstructions of hurricane activity over the past millennium from blue holes in The Bahamas include Wallace et al., 2019, 2021 and Winkler et al. (2020). Each of these reconstructions capture modern coarse-grained deposits that date to known historical hurricanes (≥Category 2 on the Saffir Simpson Scale) passing proximal to each site, which when synthesized support century-scale changes in hurricane activity over the past millennium (Wallace et al., 2021). Each island experienced extended periods of substantially elevated storm strikes interspersed with periods of relatively few TC landfalls. These reconstructions taken together allow us to better understand how hurricane activity in The Bahamas has changed over the past 1000 to 1500 years. With less than 169 years of observational data of hurricane strikes in this region (Knapp et al., 2010), these paleorecords provide one of the few means to constrain how Bahamian hurricane activity changes on long timescales (multi-decadal to centennial scale).

Constraining how these documented long-term changes in hurricane activity relate to climate is more difficult. Each single paleohurricane reconstruction only captures changes in storm activity at or near its location, which may or may not be indicative of broader variance in hurricane climate throughout the Western North Atlantic. A recent proxy-model comparison study (Wallace et al., 2020) using the South Andros paleo record (Wallace et al., 2019) and synthetic TCs generated using a statistical deterministic hurricane model (Emanuel et al., 2006, 2008) shows that the centennial-scale shifts in hurricane frequency captured in individual records from The Bahamas can be created by random variability (i.e., local weather patterns-steering winds, moist convection) not climate. To confidently identify hurricane risk for the entire Bahama Archipelago, one must compile records from across that area to better sample a representative population of storm passage. Working towards the goal of generating a large regional database of high-resolution hurricane reconstructions spanning the last millennium from the North Atlantic, here we update the paleohurricane compilations of Wallace et al. (2021) with a new high-resolution record from Middle Caicos Island.

2. Methods

2.1. Study sites

The Caicos platform, located at the southern tip of the Bahama Archipelago, is 100 km by 70 km with the northern margin exposed to the Atlantic Ocean (Fig. 1). The platform interior is sheltered predominately by a ring of islands and a barrier reef to the north. The three main land areas to the north of the platform interior are North, Middle, and East Caicos (Fig. 1). Each island is separated by tidal channels with carbonate tidal flats that extend 6 to 12 km in width on their southern margins. The Caicos platform interior extends out another ~50 km in length and the southern margin is rimmed by sand banks and patch reefs (Wanless et al., 1988a, 1988b).

About 2 km from the edge of the tidal flats (6 km from the vegetated upland) on the southern shoreline of Middle Caicos Island (at 21.72°N, 71.81°W) is a large blue hole spanning almost 0.5 km in diameter (Fig. 1). The blue hole is currently ~60 m deep while the surrounding shallow lagoon is 0–2 m deep. This interior platform shallow lagoon offers an ample supply of carbonate sediment that can be transported into the accommodation space provided by the blue hole. The surface sediment surrounding the Middle Caicos blue hole is finer grained than most other regions on the Caicos platform interior and dominated by carbonate packstone and wackestone sediments (Wanless et al., 1988a; Kaczmarek and Hasiuk, 2008). On the dates of measurement, conductivity-temperature-depth (CTD) casts in the blue hole indicate a well-defined thermocline and halocline at approximately 30 m in depth, with anoxic to dysoxic conditions for the bottom 30 m of the water column (Fig. 1). This April CTD profile is likely seasonally dependent; other blue hole basins indicate more collapsed thermoclines in the boreal winter (e.g., Wallace et al., 2021).

There are very few processes that generate onshore-directed currents towards the tidal flats of Middle Caicos Island. The Caicos platform is exposed to prevailing easterly Trade Winds and the westward-flowing Antilles Current throughout the year which run parallel to the island shore (Dravis and Wanless, 2017). This generates a westward-flowing cross-bank circulation. Winter storms typically generate offshore-directed winds, characterized by stronger winds from the northwest, north, and northeast (Wanless et al., 1988a). Since the Caicos platform is positioned along a passive margin, there has been very little tectonic activity in the area during the Quaternary period (Carew and Mylroie, 1995). Historically, no significant tsunamis have impacted the island (National Geophysical Data Center/World Data Service); only the passage of tropical cyclones can generate onshore-directed currents. TCs in the northern hemisphere are characterized by counterclockwise circular winds. Thus, TCs that pass to the north of the Caicos Islands

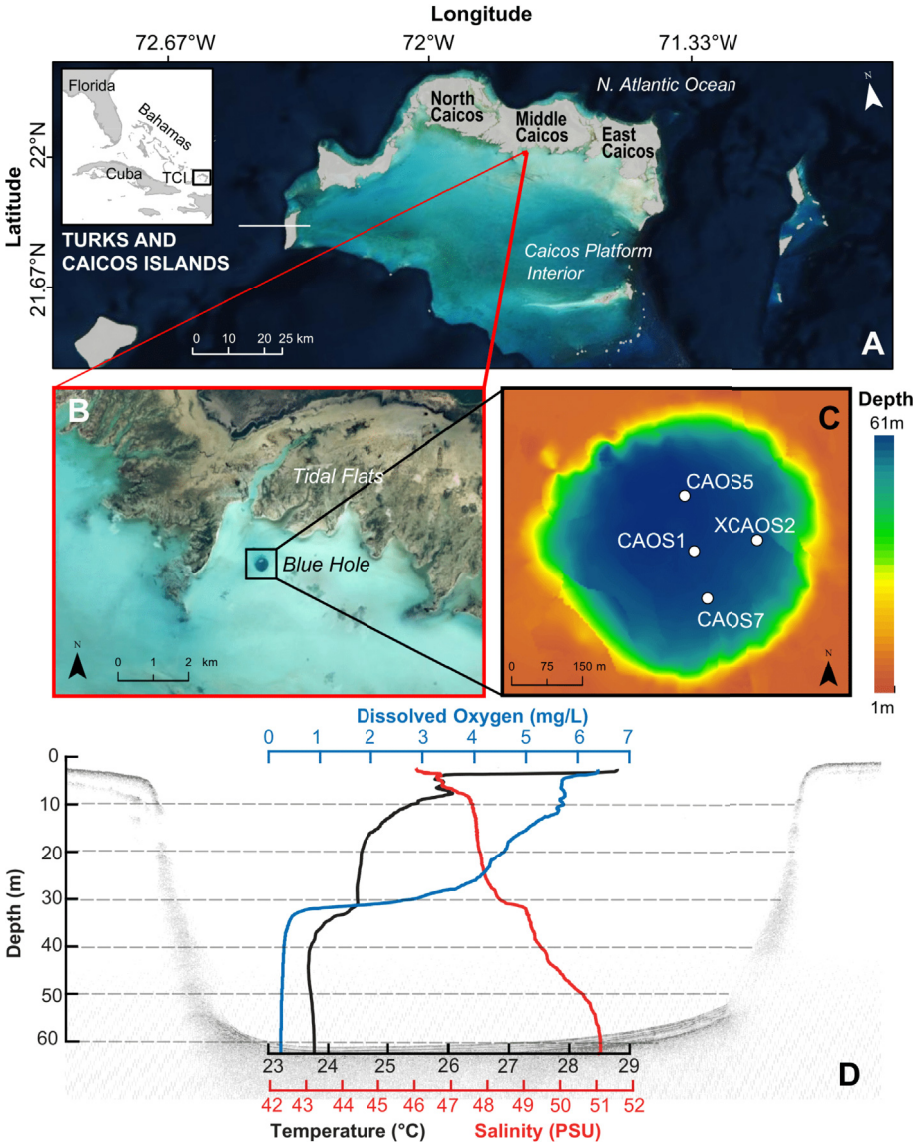

Fig. 1. (A) Map of the Turks & Caicos Island. (B) Middle Caicos Blue Hole (CAOS) location (21.72°N, 71.81°W). (C) The bathymetry of the blue hole and locations of the original 2016 transect of longer cores (CAOS7, CAOS1, and CAOS5) and post-Irma short surface core (XCAOS2) are shown. (D) Temperature (black), salinity (red), and optical dissolved oxygen (blue) profiles collected on April 27, 2016 using a YSI EXO1 sonde.

generate offshore-directed winds/currents on the Caicos platform interior during the front end of the storm and onshore-directed winds/currents for the back end of the storm. The opposite wind patterns apply for TCs that pass south of the Caicos islands.

Since 1850 CE, 62 TCs have passed either directly over or nearby (within 100 km of) the Caicos platform (Knapp et al., 2010). Only 27 of those storms had achieved hurricane strength upon closest passage to Middle Caicos with 14 of them categorized as intense hurricanes (≥Category 3 on the Saffir Simpson scale). Like many other locations in North Atlantic basin (Hall and Hereid, 2015), Turks & Caicos experienced very few intense storms in the 2010s. Hurricane Irma in 2017 was the first intense hurricane to significantly impact the island in the last decade. Irma passed approximately 75 km to the south of Middle Caicos at Category 5 strength with max sustained winds at ~140 knots and a radius of maximum winds of ~30 km. On South Caicos and Providenciales, approximately 70 % of homes were destroyed and economic losses are estimated at USD $500 million (Podlaha et al., 2018).

Several studies have investigated the Holocene sedimentary processes on the Caicos platform and the impact of recent hurricanes and tempestite formation on the subtidal carbonate lagoon (Wanless et al, 1988a, 1988b; Dravis and Wanless, 2017; Trower et al., 2018, 2019). In particular, Wanless et al. (1988a, 1988b) documented the impacts of Hurricane Kate in 1985 on the North and Middle Caicos tidal flat system. They found evidence for resuspension of finer sand and silts and strong bedload movement of coarser sands during this relatively low intensity storm. In particular, they documented storm infilling of shrimp (*Calliannassa*) burrows in the Caicos platform interior (Wanless et al., 1988a) and layers of peloidal grainstone dumped across shore levees and inland algal marshes on North Caicos (Wanless et al., 1988b). Recent field studies on Little Ambergis Cay, a small island to the south of Turks & Caicos, document small, ungraded washover fans deposited during Hurricane Irma (Jamison-Todd, 2019).

2.2. Field program

In April 2016, we used an Edgetech 3100 Chirp 4–24 kHz sonar system to map the bathymetry and sub-bottom stratigraphy of the Middle Caicos Blue Hole (referred to as CAOS hereafter). We then collected three long cores ~100 m apart along a northwest transect (CAOS7–14 m long, 21.719°N, 71.812°W ±3 m; CAOS1– 12 m long, 21.720°N, 71.812°W ±3 m; CAOS5–12.5 m long, 21.721°N, 71.812°W ±3 m) using a Rossfelder P-3 vibracore from the *RV Arenaria*, a customized 6-m pontoon vessel (Fig. 1). In addition, we collected a short (1–2 m) surface drive at each of the long vibracore locations to carefully curate the upper stratigraphy and sediment-water interface. The data from the first 39 cm, 72 cm, and 43 cm of CAOS7, CAOS1 and CAOS5, respectively, originate from their companion surface drives. Overlap between the surface drive and deeper vibracore at each core location was pinpointed using sediment textural data (i.e., coarse fraction results) and optical images from the cores (Fig. S1).

In June 2019, we returned to the site to assess the sedimentary signature left by Hurricane Irma, which passed to the south of Turks & Caicos on September 8, 2017 as a weakening Category 4 storm. We collected a short surface drive (XCAOS2, 1.3 m long) using a Rossfelder P-3 vibracore from an inflatable raft. Overlap between XCAOS2 and the surface cores from 2016 was similarly determined using both the coarse fraction data and optical images (Fig. 2). To create our final coarse fraction record, we concatenate the upper 25 cm of XCAOS2 to the top of the CAOS7 record.

2.3. Sediment analysis and event bed definition

In the field, we sectioned the long cores into 1.5 m lengths and then shipped them to Woods Hole Oceanographic Institution (WHOI) where they were split lengthwise and visually described and then photographed with an ITRAX X-ray fluorescence scanner (Fig. 2). Each core was then sub-sampled continuously at 1 cm intervals to assess the coarse fraction by dry weight following procedures described in Wallace et al. (2019). This sediment processing procedure consisted of four steps: 1) sub-sampling the core, 2) drying the samples (8 h in 100°C), 3) weighing then wet sieving the dried bulk samples at 63 μm, and 4) drying and weighing the retained coarse fraction.

Textural variability in the CAOS cores alternates between laminated fine-grained carbonate mud and thick coarse-grained (predominantly very fine sand to coarse sand sized) beds (Fig. 2). We distinguished event beds from the background fine-grained sediment in the longest core CAOS7 using the optical scans and the coarse fraction data. All event beds must 1) be visually distinct from the background sediment and 2) contain a peak in the coarse fraction data. The background sediment is light grey (Munsell color 2.5Y 8/1) with white (Munsell color 7.5 YR 8/0) and dark brown (Munsell color 5 YR 6/2) laminations (Fig. 2). These laminations are likely caused by changing organic matter content within the cores resulting from variation in surface water productivity (Gischler et al., 2008; Denommee et al., 2014). Visual cues for event beds include lighter cream-colored sediment (Munsell color 5 YR 8/2) topped with darker tan colored (Munsell color 5 YR 7/2) sediment, visibly coarser grains, higher concentrations of organics, and no laminations. Event beds have sharp defining visual contacts that were used to delineate the starting and ending point of each event bed (Fig. 2). Coarse fraction peaks in CAOS7 were identified by setting an event coarse anomaly threshold (Donnelly et al., 2015). This threshold is defined in two steps: 1) Calculate the coarse anomaly using a 10-point moving filter from the data (excluding coarse fraction peaks over 25%), and 2) pinpoint coarse anomaly peaks that exceed two sigma of the cumulative distribution function of the data over the observational interval (1851–2019), which in the case of CAOS7 was determined to be 17.5% (Fig. S2). Event beds in the longest core, CAOS7, were then stratigraphically traced across the transect of cores (i.e., in CAOS1, in CAOS5) (Fig. 3).

2.4. Chronology

Plant macrofossils from all three cores were pulled and radiocarbon dated at the National Ocean Sciences Accelerator Mass Spectrometry Facility (NOSAMS) at WHOI: 18, 2, and 20 samples from CAOS7, CAOS1, and CAOS5, respectively (Tables S1 and S2). We include dates from CAOS5 and CAOS1 in our depth-to-age model for CAOS7 (Fig. 4) based on depth referencing to correlative stratigraphy traced between cores (i.e., visual, sedimentological). The organic remains dated in only 14 of our radiocarbon samples (Table S1) have stable carbon isotopic ratios ($\delta^{13}C_{org}$) that commonly characterize organic carbon generated by terrestrial C3 plants (−20 to −30 ‰ - Kohn, 2010). The other 26 samples have more enriched $\delta^{13}C_{org}$ values, ranging from −5.4 to −14.4 ‰ (Table S2). Such enriched $\delta^{13}C_{org}$ values are typically associated with CAM or C4 plants, which includes aquatic macrophytes and algae (Deines, 1980; Wefer and Killingley, 1986; Duarte et al., 2018). It is difficult to accurately calibrate radiocarbon dates derived from marine plants and algae as they take in at least some of their carbon from oceanic sources. Marine carbon is subject to a 'reservoir effect' related to the residence time of carbon cycled in the ocean, meaning that these marine organisms often take in "older" carbon sources that result in radiocarbon dates older than the organism itself (Deines, 1980). Indeed, many of our results with more enriched $\delta^{13}C_{org}$ values are ~400 years older than the lower $\delta^{13}C_{org}$ samples associated with terrigenous C3 plants (Fig. S3). Unfortunately, since the reservoir correction varies quite dramatically throughout the ocean and we were not able to identify exactly what type of plant material we dated (Supplemental Section S1), we could not accurately reservoir correct these samples. Therefore, we excluded radiocarbon results with more enriched $\delta^{13}C_{org}$ values in our final age model determination (Fig. 4).

Our depth-to-age model consists of 11 dates over 867 cm (Fig. 4 and Table S1) that was calculated in Bayesian accumulation (BACON) histories for deposits software version 2.5.2 (Blaauw and Christen, 2011). All the dates were calibrated using IntCal20 (Reimer et al., 2020). While the age model output from BACON was resolved to 1 cm core depth increments, we recognize that tempestites thicker than 1 cm were deposited near instantaneously. As such, we removed all event beds prior to age modeling by representing them as a 'slump' in BACON (Rodysill et al., 2020; Winkler et al., 2020). Afterwards, all event beds were condensed down to 1 cm in thickness and reinserted following age-depth estimation. We excluded three additional dates that did not exhibit the enriched $\delta^{13}C_{org}$ signature (Fig. S3), because they were not chronologically consistent with the rest of the dating evidence.

2.5. Event thresholds and frequency

We calculated event frequency per century in a 100-year moving window using the event beds in CAOS7 (Fig. 5). We define active and quiescent intervals using established methods (See Lane et al., 2011). Assuming event occurrence follows a Poisson process, we estimate a site-specific expected event frequency. Given that 74 storms left deposits in the CAOS7 core over the past 1520 years, we compare time varying changes in event frequency in the CAOS7 reconstruction to the average event frequency, 4.9 events/century, obtained over the entire record. We calculate that the 90 percentile upper confidence bound (Ulm, 1990) above our expected 4.9 events/century frequency is 5.9 events/century. Active intervals are

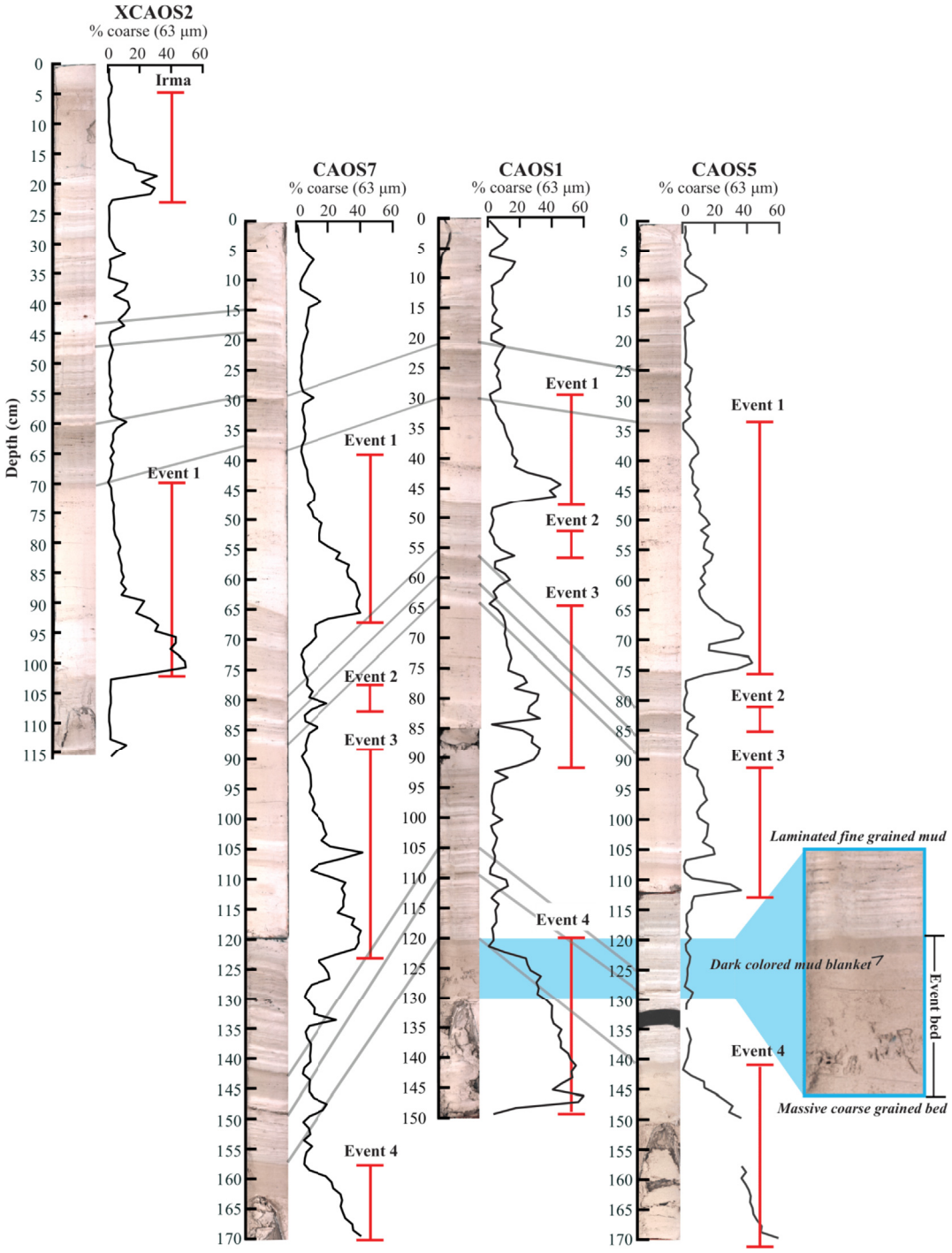

Fig. 2. Optical images from the ITRAX X-ray fluorescence scanner and coarse fraction (>63 μm) data of the shorter surface drives from XCAOS2 (collected in 2019) and CAOS7, CAOS1, and CAOS5 (collected in 2016). Visual event beds (Events 1–4) are denoted by the vertical red bars and labels. The top of Event bed 4 in CAOS1 is highlighted. Visual cues for event beds included: lighter colored sediments topped with darker colored sediment, visibly coarser grains, higher concentrations of organics, and no laminations. Lines of correlation (grey) are drawn between cores matching up the same sets of laminations in each core. XCAOS2 (far left) includes an event bed in the top 25 cm not found in any of the other 2016 cores that we attribute to Hurricane Irma in 2017. Inclined stratigraphy in the CAOS7 surface drive shown is not present in the longer drive and likely resulted from coring at a slight angle.

extended periods of time when the 100-year window frequency exceeds this upper confidence bound (Fig. 5).

Quiescent intervals, on the other hand, are defined using methods established in Wallace et al. (2019). We set the recurrence interval for hurricane strikes at the CAOS blue hole to 20.5 years/event using 74 storms that left a deposit in CAOS7 over the whole record (498–2019 CE). Quiescent intervals are extended time periods (>50 years) in the record when 1) no events occur and 2) the probability of having no events over that extended time period is low (below 50%) (Fig. 5).

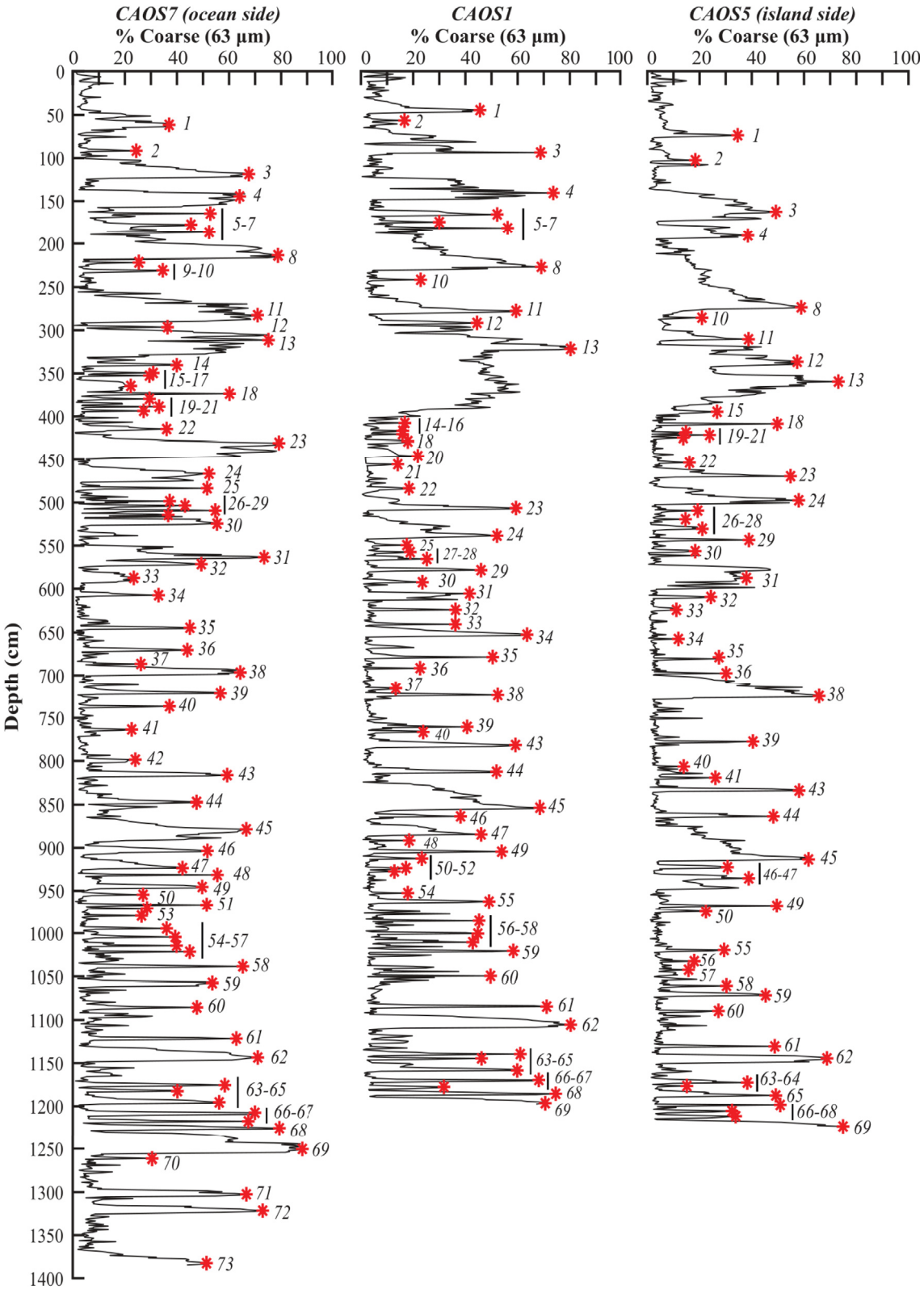

Fig. 3. Depth profiles of percent sand fraction (>63 µm, black) for CAOS7 (left), CAOS1 (middle), and CAOS5 (right). Event beds (red stars) were identified using visual cues and correlated across cores (See Fig. 2). Event beds are numbered from 1 to 73 on the CAOS7 core (the Hurricane Irma layer from XCAOS2 is not plotted). The same event beds found in CAOS7 are labelled in CAOS1 and CAOS5, but CAOS1 and CAOS5 only include 62 and 53 events, respectively.

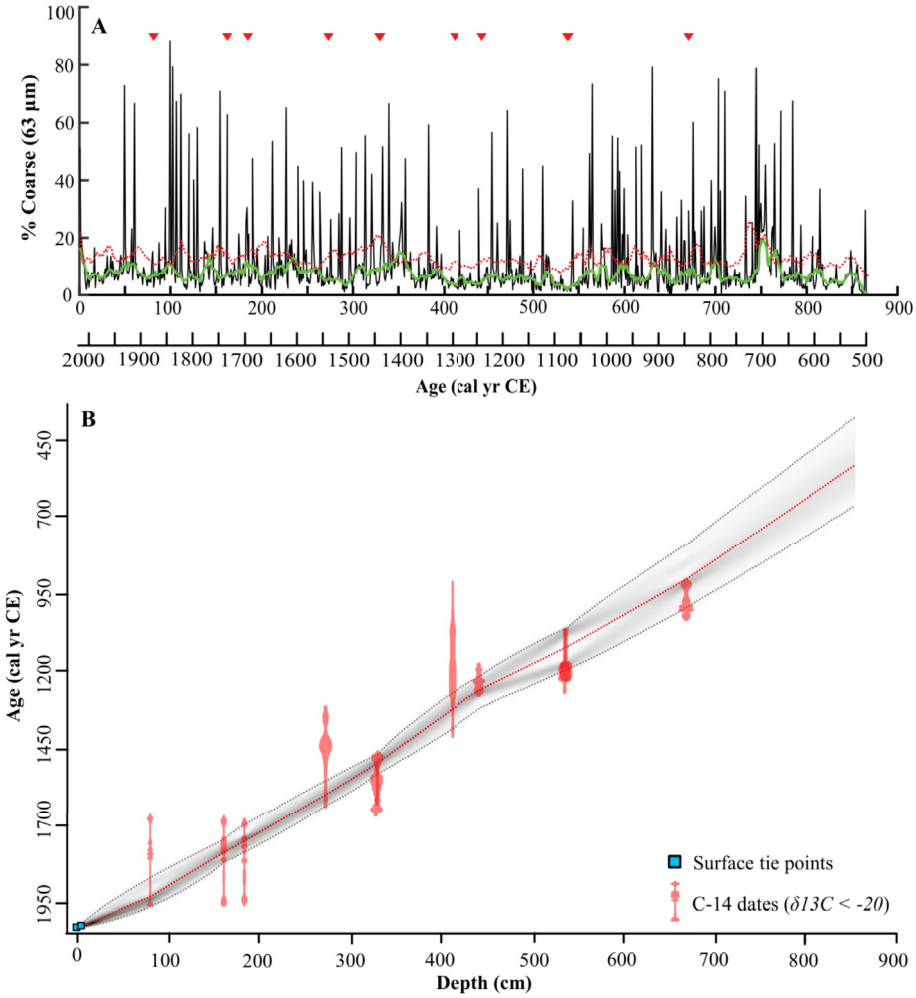

Fig. 4. (A) Depth profile of percent sand fraction (>63 µm, black) from CAOS7 with a 10-point running mean filter (green) that excludes coarse fraction values above 25%. The red dashed line is the 95% event cutoff threshold added to the filter. Depths of ^{14}C dates are plotted as red triangles. Secondary x-axis below A of age is derived from the age model shown in B. (B) Age model (red dashed) derived from radiocarbon dates (red) in Table S1 for CAOS7. Radiocarbon samples were pulled from CAOS5 and CAOS7; all depths in CAOS5 were referenced to CAOS7. There are two overlapping dates (one from each core) shown at ~330 cm and ~540 cm. 95% confidence bounds are shaded in grey. Two tie points setting the surface of each core to year of collection (2019 and 2016) are also shown (teal boxes). This figure was generated using BACON v2.5.2 age modeling software (Blaauw and Christen, 2011).

3. Results

3.1. Seismic stratigraphy and correlating event beds across cores

The seismic stratigraphy in the CAOS blue hole reveals only 1–2 m of penetration before the acoustic signal attenuates in gas in the pore space of the sediment. The seismic reflection survey profiles (Fig. 6) show steeper edges with a gently sloping basin floor. The CAOS blue hole shallows towards the ocean side of the basin (i.e., southeast side) likely as a consequence of predominant sediment infilling from the ocean side (Gischler et al., 2013). In the resolved upper 1–2 m of the sub-bottom stratigraphy, there are several continuous draping layers of sediment that extend throughout the subsurface. High amplitude reflections in the profiles delineate alternating layers of fine- and coarse-grained sediments. There is no evidence in the seismic reflection survey results for bioturbation, thickening/thinning of the high-density reflectors in the subsurface, complex crossbedding from wave-induced sediment transport from bottom currents or attenuating high-density reflectors in geographic space that would potentially indicate lobe-shaped tempestites in the basin.

Seventy-four event beds were identified in CAOS7, and all but three of those event beds were identified in at least one other core in the transect. Over the top 1255 cm, we identified 69 events in our most seaward CAOS7 core, 62 at the middle CAOS1 site, and 53 of them in the most landward CAOS5 location (Fig. 3). All event beds identified in either CAOS1 or CAOS5 were visually correlated to a bed in CAOS7. The decrease in overall number of event layers when progressing from ocean (CAOS7) to landward (CAOS5) cores is consistent with a predominant seaward source of sediment for these events. This notion is supported by an increase in the overall depositional package towards the ocean side of the blue hole (Fig. 6). As CAOS7 contains the longest record of events striking the site, we used the event beds identified in the CAOS7 core to establish the temporal frequency of events on Middle Caicos.

3.2. Event bed properties and event frequency patterns

The CAOS7 core exhibits a relatively uniform average sedimentation rate at approximately 0.6 cm/year (Fig. 4). We identified 74 event beds over the past 1520 years (Fig. 5). The thickness of event beds varies from 1 to 100 cm with average coarse bed

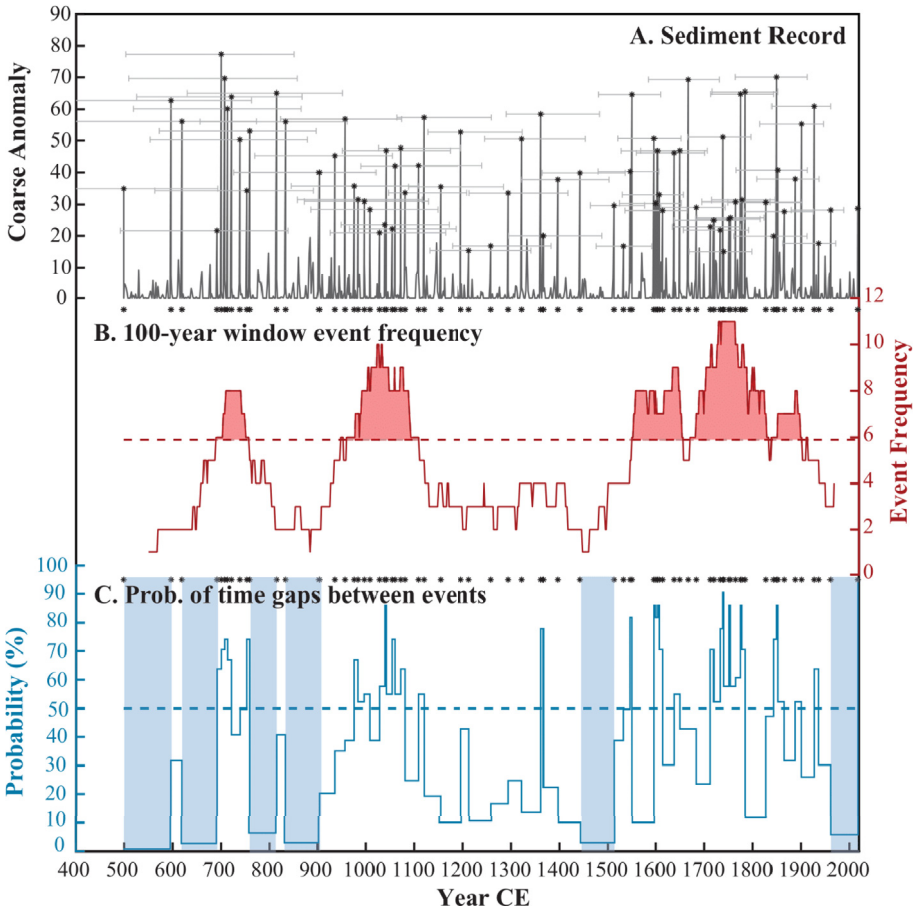

Fig. 5. (A) Coarse anomaly plot (grey) for CAOS7 as a function of time. Black starred peaks are counted as event beds using both the optical images and coarse fraction data. Grey error bars indicate 95% confidence bounds for the ages of each event. (B) The 100-year moving window event frequency per century. The dashed red line is the site-specific 90th percentile cutoff for active intervals (5.9 events/century). (C) The probabilities of having no events over the time span between each event in the record. The probabilities were calculated based on a recurrence interval of 20.5 years/event over the whole record (blue). Active and quiet intervals identified on Middle Caicos are shaded in red and blue, respectively.

thickness at 7.7 cm. Most coarse beds in CAOS7 exhibit a fining upward sequence with many of the thicker event beds featuring larger (~1 mm) white shell fragments that are concentrated at the bottom of the bed.

While all these event beds were visually distinct from the background sediment, only 70 of the 74 events showed a corresponding peak in the coarse anomaly data above the two-sigma 17.5% threshold. Given that these beds involve a peak in coarse fraction, can be visually distinguished in CAOS7, and tracked across a transect of cores, we argue that they do in fact represent storm deposits. The addition of these four events to the record does not create significant differences in event frequency patterns (Fig. S2).

We identify three multi-decadal active periods on Middle Caicos over the past 1520 years (as defined by the 100-year window event frequency) from 690 to 760 CE, 960 to 1100 CE, and 1550 to 1900 CE. (Fig. 5). The period with the highest activity on Middle Caicos over the past 1520 years is from 1550 to 1900 CE with an average event frequency of 8.0 events/century. These active periods are replicated in the 50-year window event frequency (Fig. S4). Middle Caicos also experienced extended time periods where no storms left deposits. We found six such quiescent periods from 498 to 595 CE, 618 to 690 CE, 758 to 813 CE, 831 to 901 CE, 1444 to 1514 CE, and 1961 to 2017 CE (Fig. 5).

4. Discussion

4.1. Site-specific considerations on Middle Caicos

Our transect of long cores across the CAOS blue hole allows us to assess both the vertical and lateral sorting of tempestites across the widest Atlantic blue hole cored to date (0.5 km diameter). The stratigraphy from our transect suggests continuous settling of coarse-grained sediment across the blue hole. Given the shallowing in the blue hole bathymetry towards the ocean (southeast) side of the basin (Figs. 1 and 6), it is likely that sediment infills predominantly on the ocean side, but during a storm event, coarse-grained sediment can be transported as far as 350 m (CAOS5) from the blue hole edge. 70% of the tempestite layers found in the ocean-side core (CAOS7) were also recovered in both the middle (CAOS1) and island-side (CAOS5) cores (Fig. 3). Finding more deposits in the ocean-side core (CAOS7) offers evidence for some lateral sorting of and/or spatially restricted event sedimentation in the CAOS blue hole. However, we do not find evidence for 'lobe-like' tempestites like those found in Lighthouse Reef blue hole in Belize (Schmitt et al., 2020) in our stratigraphy (Fig. 6). There is also no consistent pattern of decreasing bed thickness if we follow the same event bed across cores in the transect moving from ocean to island

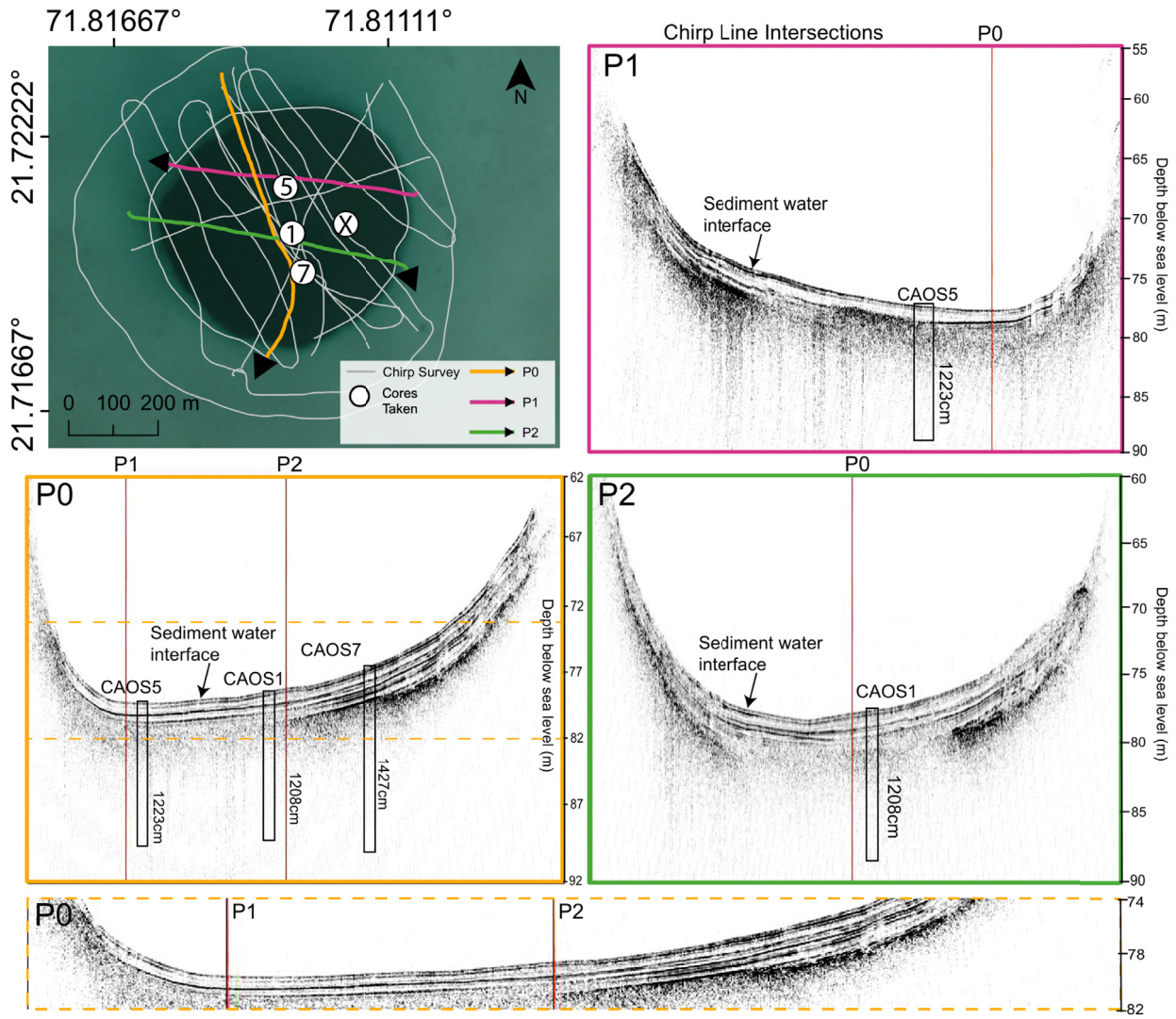

Fig. 6. (A) Satellite image of the CAOS blue hole including Chirp track lines and core locations (7-CAOS7, 1-CAOS1, 5-CAOS5, X-XCAOS2). (P0–P2) Sub-bottom stratigraphy taken with the Edgetech 3100 Chirp sub-bottom sonar system in 2016 for colored track lines in panel A. The seismic velocity was set at 2000 m/s (Anselmetti and Eberli, 1993). Approximate core locations are shown on P0–P2 panels with original core lengths indicated by rectangles. Vertical lines show intersecting track lines. In each panel, the lateral continuity of horizontal reflectors in the sub-bottom suggests continuous fine-grained layers interspersed with coarser layers (event beds). The seismic signal is obscured by the presence of gas approximately 2–3 m below the sediment-water interface.

side. However, evidence for spatially restricted event beds found both in our cores in Middle Caicos and cores from Lighthouse Reef blue hole (Schmitt et al., 2020) highlights the importance of collecting/comparing several cores when creating high resolution paleohurricane records in blue holes. Future researchers cannot necessarily assume that all blue hole event layers are deposited as a uniform drape of sediment across the basin such that a single core from a basin will capture all event layers.

The vertical thickness of tempestites in the CAOS cores speaks to the volume of sediment (both fine- and coarse-grained) that is suspended and transported and then gradually settles on the Caicos platform after storm events. We observed multiple unusually thick tempestites (40–100 cm thick) in the CAOS cores characterized by a distinct fining upward sequence. Many of these thick deposits contained darker colored fine-grained sediment blankets at the top ranging from 1 to 6 cm in thickness (Fig. 2). All other existing blue hole records (i.e.,Wallace et al., 2019, 2021; Schmitt et al., 2020; Winkler et al., 2020) capture coarse deposits less than 30 cm in thickness with the vast majority of deposits in the 1–5 cm range. There are many different potential controls on event bed thickness including coarse-grained sediment availability as well as storm properties like return period, intensity, and duration. A more intense and slower-moving storm might transport more sediment into a blue hole basin. Storm return period can impact sediment availability. If storms occur too frequently, there is less time for reefs to recover and thus lower abundance of erodible reef material. Climate in the Caribbean, however, is generally favorable for hurricane formation and intensification. Thus, it is unlikely that any existing blue hole site has seen preferentially more frequent, slower-moving, or more intense TCs. Therefore, we argue that the CAOS blue hole record exhibits thicker storm deposits because the Caicos Platform is not coarse-grained sediment limited. The Caicos platform interior, unlike many other existing blue hole sites, features many active depositional environments including two shoals (Kaczmarek and Hasiuk, 2008) that provide an ample supply of coarse-grained sediment that can be transported across the platform during storm events. Indeed, local pilots observed suspended plumes of mud and low visibility on the Caicos platform over 15

days after the passage of the low intensity Category 1 Hurricane Kate in 1985 (Wanless et al., 1988a).

Despite abundant local sediment supply on the Caicos platform, the sediment accumulation rate (0.6 cm/year) without event bed sedimentation in the CAOS blue hole is on the lower end of sedimentation rates found at other Atlantic blue hole sites (i.e.,Wallace et al., 2019, 2021; Schmitt et al., 2020; Winkler et al., 2020). Many of the smaller blue holes from The Bahamas (max diameter 150 m; max depth 90 m) have higher sedimentation rates ranging from 0.9 cm/year (South Andros blue hole (AM2), The Bahamas - Wallace et al., 2019) to 1.6 cm/year (Thatchpoint Blue Hole, The Bahamas - Winkler et al., 2020). Larger blue holes like Lighthouse Reef Blue Hole in Belize (max diameter 350 m; max depth 125 m) have lower sedimentation rates (0.25 cm/year) (Schmitt et al., 2020) similar to the CAOS blue hole. In addition, site-specific geomorphology can also play an important role in lowering sedimentation rates in a blue hole basin. At Lighthouse Reef, a surrounding coalesced coral reef causes baffling and trapping of coarser sediments and a gentle (30°) sediment slope on the blue hole supports deposition (Schmitt et al., 2021). These geomorphic features are not present in many of the other smaller blue holes that are located in lagoons (Winkler et al., 2020; Wallace et al., 2021) or tidal channels (Wallace et al., 2019). As more blue holes are explored, future work should investigate how blue hole geometry and geomorphology relates to sediment accumulation rates.

It's important to acknowledge that the age model for the CAOS7 record is much more uncertain than other previously published blue hole records. Most of the dates (10 of 11) in our chronology are concentrated in the top 540 cm. This leaves only a single radiocarbon date for the bottom 320 cm of the core. Therefore, we expect that the oldest 24 events in the record are much more uncertain than younger events due to greater extrapolation of the age model. More work is needed creating marine reservoir corrections for different islands/regions in the Caribbean before we can confidently correct the marine contaminated samples collected in our cores for use in the age model.

4.2. Event attribution during the historical period

To assess the sensitivity of our Middle Caicos blue hole sediment reconstruction to different types of passing hurricanes, we investigate which recent storms have left coarse event beds in our sediment cores. Over the observational period, 27 hurricanes (Category 1 and above) have passed within 100 km of the CAOS blue hole (Fig. 7a). Most of these storms (23 of 27) can be characterized as Cluster 3 or 4 storms (Kossin et al., 2010) that form far to the southeast of the site off the west coast of Africa ('Cape Verde' hurricanes) or in the Main Development Region to the east of the Lesser Antilles (Fig. 7b) and pass the Caicos platform in a southeasterly direction. The other four storms are Cluster 1 storms (Kossin et al., 2010) that form in the northeastern Atlantic and often recurve away from the U.S. East Coast. Of these 27 historical storms, 11 storms passed to the south of the site. The other 16 passed to the north or west (Fig. 8).

We argue that TCs passing to the south of Turks & Caicos are better suited to generate on-shore directed sediment transport and leave the coarse-grained deposits we find in the CAOS blue hole cores than their northward-passing counterparts. The North, Middle and East Caicos islands shelter the CAOS blue hole from storms passing to the north (Fig. 9). Northward-passing TCs generate offshore-directed winds on the Caicos platform interior as the front end of the storm passes. The wind patterns switch as the back end and less intense part of the storm passes (rear left quadrant) over the site. How the back end onshore directed winds translate into storm surge and increased wave height depends on the size and forward speed of the storm and its distance from the site. If the storm passes close enough to the site that the radius of maximum winds (RMW) falls over the Caicos platform interior, there is more likely to be increased wave energy and onshore bottom currents than if the storm passes too far away for its RMW to intercept the platform interior.

When TCs pass to the south of Turks & Caicos, on the other hand, the front right and most destructive quadrant of each storm impacts the CAOS blue hole (Fig. 9). These southward passing TCs generate the strongest onshore directed winds piling water on the southern side of Middle Caicos Island. Southward passing storms also generate larger waves. Wave height is affected by the fetch or the distance over water that wind blows in a single direction. Waves generated from storms passing to the south of the Caicos Islands will travel over the entire distance of the Caicos platform uninterrupted. Waves from northward passing storms will only have a fetch equal to how far the storm wind field extends over the Caicos platform.

CAOS7 includes nine coarse event beds that date within uncertainties to the observational period (1851 to present) (Fig. 10). The average age uncertainty for each of these events is ±42 years. With the high density of storms that have passed the Caicos platform in the past century and a half (Fig. 8) and the high age uncertainty associated with each event, it is very difficult to tie each coarse bed to a single storm event with a high degree of confidence. Fortunately, we collected surface sediment cores from the Middle Caicos blue hole in 2019, after Hurricane Irma's passage in 2017. The surface core (XCAOS2) contains a single new event bed starting at 3 cm down in the core and extending approximately 21 cm in depth. Only two storms (Hurricane Irma and Hurricane Maria in 2017) passed within 100 km of Turks & Caicos from 2016 to 2019 CE (Figs. 7 and 10, Table S3).

Hurricane Irma passed 65 km to south of the Turks & Caicos Islands with max sustained winds greater than 70 m/s (Cangialosi et al., 2018). The front right quadrant of the storm swept over the Caicos islands for over 2 h. Unfortunately, observing systems on the islands failed during the peak of Irma, but reports from the island indicated extensive property damage and flooding (Cangialosi et al., 2018). Hurricane Maria, on the other hand, passed approximately 96 km to the northeast of the Caicos platform at Category 3 strength. Middle Caicos was well outside Maria's RMW (~46 km); an observing station on Providenciales recorded maximum sustained winds at 21 m/s with 25 m/s gusts. Damages reported on Turks & Caicos during Maria were minimal (Pasch et al., 2019). Therefore, we attribute Event bed 1 to Hurricane Irma (Table S3). Hurricane Irma provides a modern analog that supports the hypothesis that proximal passing storms moving to the south of Middle Caicos generate coarse beds in the CAOS blue hole.

The second and third event beds occur from 48 to 66 cm and 88 to 92 cm into CAOS7 and date to the mid to late 20th century (Table S3). Four hurricanes passed within 100 km of Middle Caicos from 1940 to 1985 CE: Hurricane Kate in 1985, Hurricane Donna in 1960, Hurricane Betsy in 1956, and a 1945 Category 3 hurricane (Table S3). Both Hurricane Donna 1960 and Betsy 1956 passed <50 km to the north of the CAOS blue hole (Fig. 8). Neither Donna nor Betsy have recorded RMW values as they passed Turks & Caicos. However, there is little evidence for significant destruction from Hurricane Donna in this region. Observations from Grand Turk suggest relatively modest maximum sustained winds (23–25 m/s) during the peak of Donna, similar to the winds observed during the passage of Hurricane Maria. Most of the observed damages were a result of rainfall-related flooding (Dunn, 1961). Sheltered by northward-facing reefs and islands, we argue that it is unlikely that the platform interior including the CAOS blue hole was significantly impacted by either Donna or Betsy.

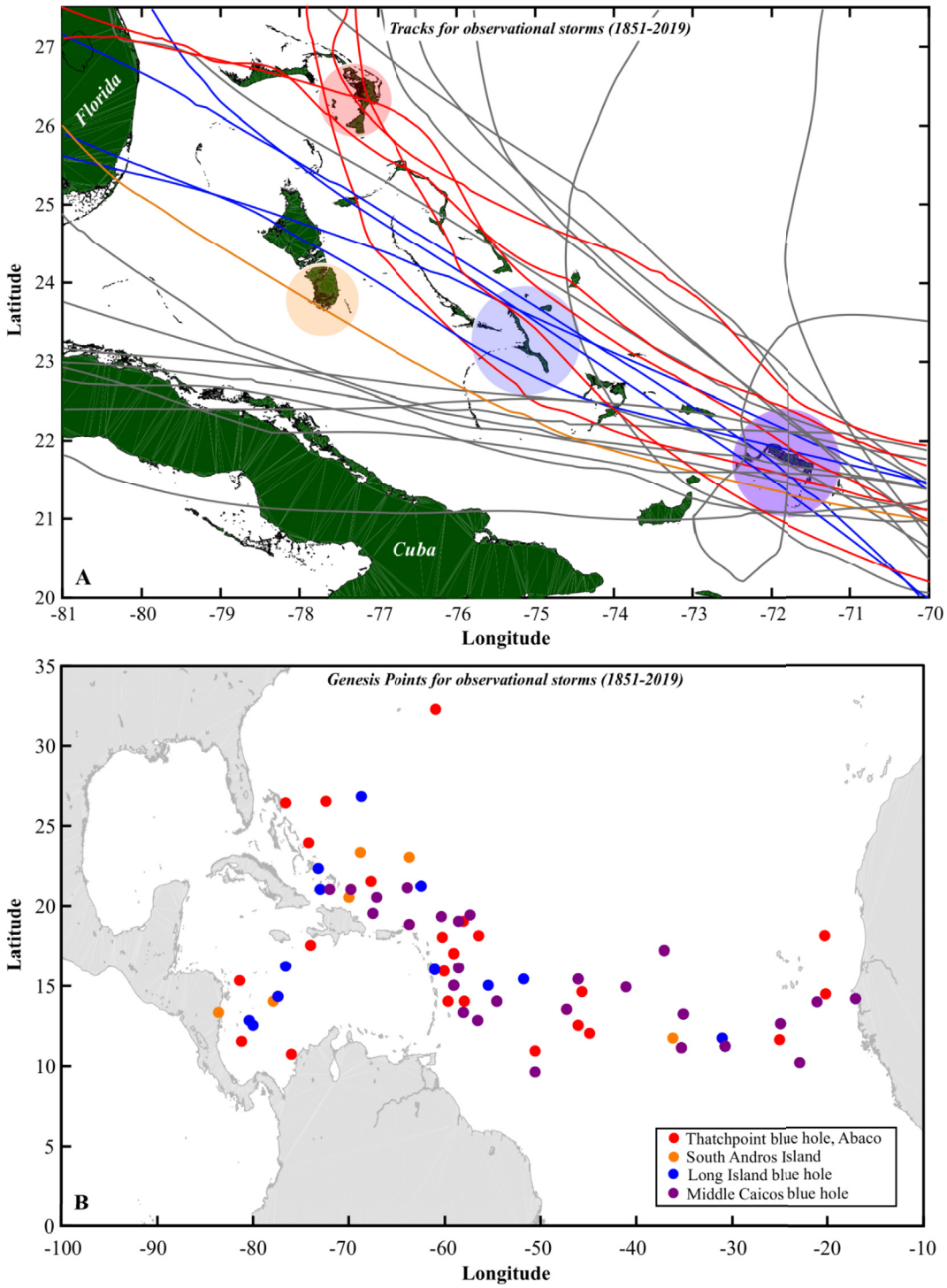

Fig. 7. (A) Map showing 50 km radii around Thatchpoint Blue Hole on Abaco Island (Winkler et al., 2020) (red) and the AM4 blue hole on South Andros Island (orange) (Wallace et al., 2019) and 75 km radii around Long Island blue hole (blue) and Middle Caicos blue hole (purple). Historical hurricane tracks (Category 1–5 from 1851 to 2019) passing within 100 km of the Middle Caicos blue hole are plotted. Storms that pass within the radii around of Abaco Island, South Andros, and Long Island are plotted in red, orange, and blue, respectively. All other storm tracks are plotted in grey. (B) Genesis points for observational storms (1851 to 2019) that passing within 75 km of Middle Caicos (purple) and Long Island (blue) and 50 km of South Andros (orange) and Abaco Island (red).

Therefore, we attribute Events 2 and 3 to Hurricane Kate in 1985 and the 1945 Category 3 storm (Table S3). Both storms passed >50 km to the south of Middle Caicos over the platform interior. Hurricane Kate was only Category 1 strength as it passed Turks & Caicos, but there is a wealth of empirical evidence for both coarse and fine sediment suspension during its passage. Wanless et al. (1988a) observed that wave action during Kate in 1985 scoured the bottom, caused resuspension of the finer sands and silts, and caused bedload transport of coarse sediments around North and Middle Caicos. In particular, the authors observed widespread flattening of burrowing shrimp mounds and infilling of burrow holes post-Hurricane Kate (Wanless et al., 1988a). They also found small coral head patches with skeletal gravel built up against the southern sides suggesting high volumes of moving sediment driven

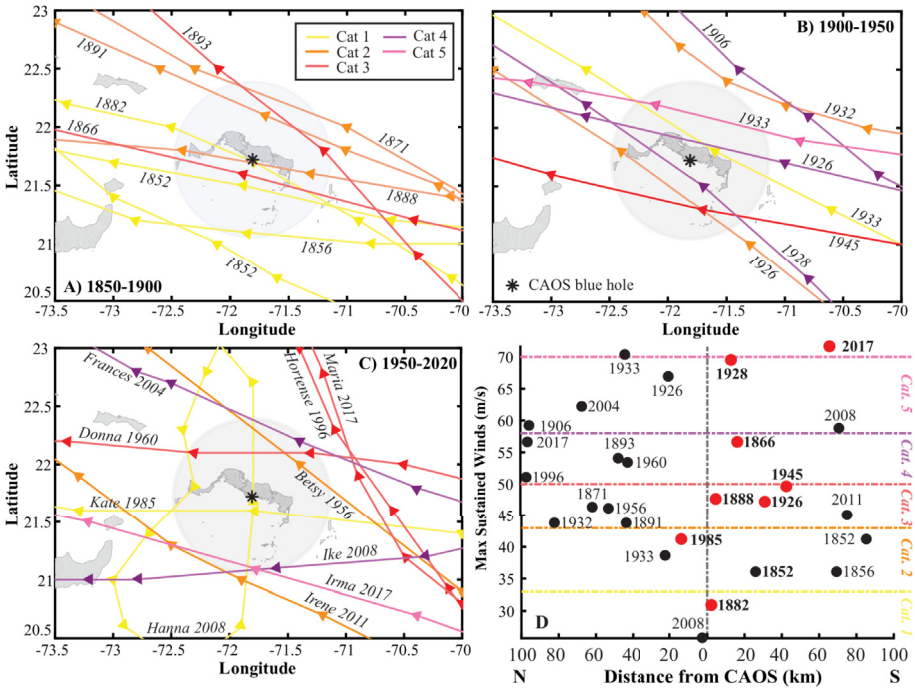

Fig. 8. Historical hurricane tracks passing within 100 km of the Middle Caicos blue hole (21.72°N, 71.81°W) from (A) 1850 to 1900 CE, (B) 1901 to 1950 CE, and (C) 1950 to 2019 CE. A black star indicates the blue hole location, and a grey circle shows a 75 km radius around the blue hole. (D) Storm intensity and orientation upon closest passage to the Middle Caicos blue hole. Red dots indicate the storms that probably left deposits in the blue hole. The storm's closest passage to the Middle Caicos blue hole is plotted to the left of zero if the storm moves to the north of the site and to the right of zero if the storm moves to the south of the site.

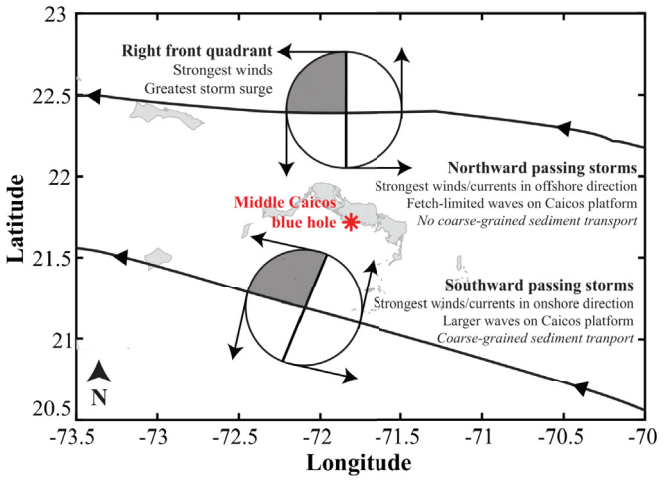

Fig. 9. Schematic of the impacts of northward passing hurricanes versus southward passing hurricanes on the Middle Caicos blue hole. Example hurricane tracks are plotted with arrows indicating the forward direction of storm. Circles indicate radius of maximum winds (~40 km) of each storm. The front right quadrant of the hurricane is shaded in grey.

by northerly winds. Further studies observed a 3–10 cm thick sediment layer characterized by 100–400 μm sized grains deposited on the subtidal ramp on the east and southeast facing shorelines of North and Middle Caicos (Wanless et al., 1988b).

The next two event beds (Events 4 and 5) are placed at 101 to 123 cm and 137 to 156 cm. They date to the early twentieth century (Table S3). Seven hurricanes passed with 100 km of Middle Caicos from 1900 to 1940 CE (Table S3, Fig. 8). Only two of these storms passed to the south of Middle Caicos Island. The 1928 Category 4 storm, also known as 'The Great Okeechobee Hurricane', passed across the Caicos platform interior moving to the north-west. Much like Hurricane Kate in 1985, it passed within 12 km of the CAOS blue hole but this time at Category 4 strength with wind speeds up to 69 m/s. Observations from after the storm suggest that most of the Caicos Islands were wiped clean of vegetation, and there was significant damage to most buildings on the islands (Neely, 2014). We attribute Event bed 4 to the 1928 Great Okochobee hurricane. We attribute Event bed 5 to the only other storm that passed to the south of Middle Caicos in the early 1900's: the 1926 Category 2 July hurricane. This storm followed a similar trajectory to the 1928 hurricane (Figs. 8 and 10). It moved northwest across the Caicos platform passing within 30 km of the CAOS blue hole with wind speeds reaching up to 47 m/s.

All of the other storms approaching Turks & Caicos in the early 20th century passed on the northern side of the Caicos Island with varying levels of storm intensity and distance from the blue hole site (Table S3, Figs. 8 and 10). Only the two 1933 storms and the 1926 Category 4 storm passed <50 km to the north of Middle Caicos. In the case of these three storms, it is possible that their RMW passed over the CAOS blue hole and the back end of each of these storms generated onshore directed currents. Given that the northward facing reefs and islands protect the platform interior and that northward passing storms generate fetch-limited waves, we think it is unlikely that these storms generated as much surge and sediment transport on the south side of Middle Caicos as their southward passing counterparts (i.e., 1928 Great Okochobee hurricane, 1926 Category 2).

The last four modern event beds (Events 6 to 9) date to hurricane events passing Caicos in the second half of the 19th century (Table S3). Event beds 6 to 8 range from 1 to 2 cm in thickness and are only recorded in the front two cores of our transect (CAOS7 and CAOS1). Event bed 9, on the other hand, has a very different character. It extends 28 cm in thickness and is captured in all three cores. All of these later event beds have larger age uncertainties (Table S3), and there is the increased uncertainty in the

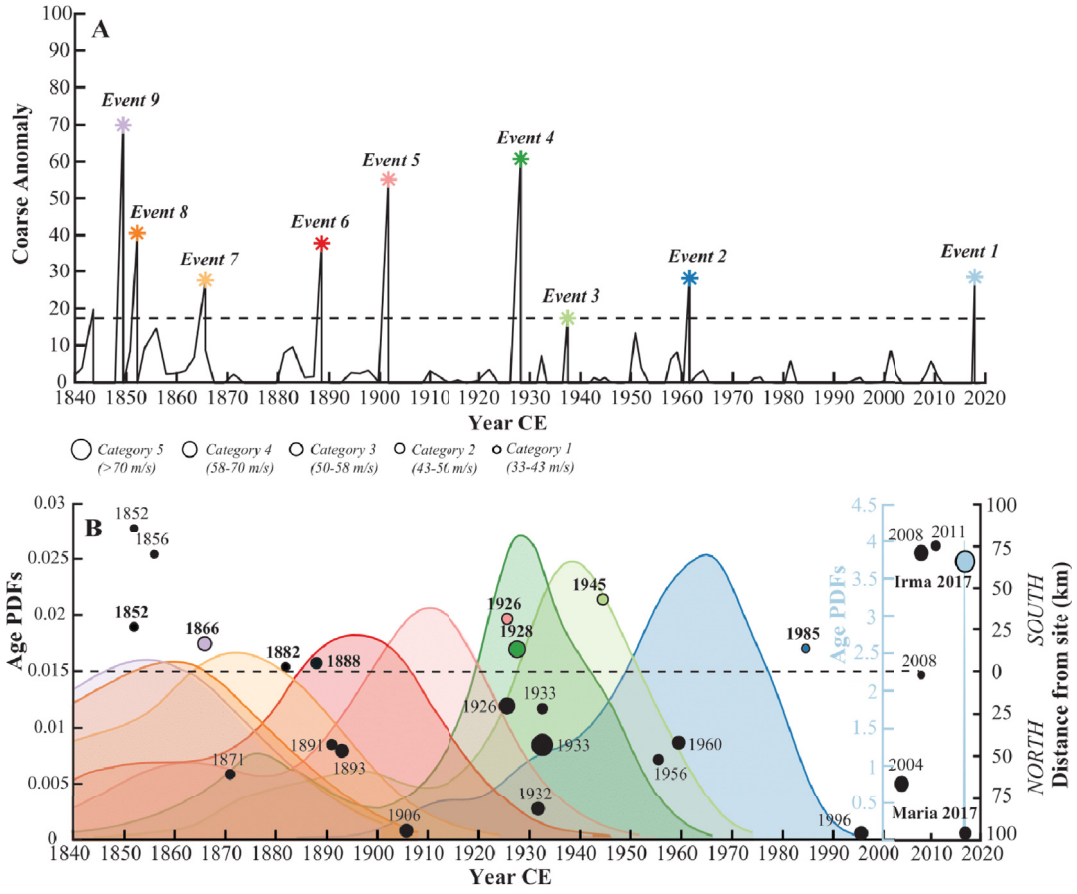

Fig. 10. (A) Coarse anomaly data from 1840 to 2019 from CAOS7. Starred peaks indicate identified event layers. (B) 95% age probability distributions for Events 1–9. Circles on panel B indicate the year observed storms passed within 100 km of the CAOS blue hole plotted as a function of their distance (km) from the site at the time of closest passage. The dashed black line marks passage directly over the site. Circles plotted above (below) the line are storms that passed to the south (north). The colored dots indicate the observational storms to which we attributed each event bed shown in panel A. The size of each circle indicates the max intensity (Category 1–5 on the Saffir Simpson Scale) of its respective modern storm when passing within 100 km of the site.

observational hurricane records prior to the 1900s (Vecchi and Knutson, 2011); thus, we cannot reasonably attribute each of these event beds to individual passing storms. From 1851 to 1900 CE, six hurricanes passed on the southern side of Middle Caicos Island (Table S3, Fig. 8). Most of these storms (i.e., 1888 Cat. 1, 1882 Cat. 1, 1852 Cat. 1) moved within 50 km of the CAOS blue hole at low intensity (Fig. 8). It is likely that some of these less intense southward passing storms created event beds 6–8. Of these storms, only one was categorized as an intense hurricane. The September 1866 hurricane passed about 16 km to the south of Middle Caicos at Category 3 strength (Fig. 10). Almost 75% of the country's population was left homeless, and all of the industries including fishing, sea salt production, and cotton and sisal cultivation were devastated after this hurricane (Neely, 2006). We attribute Event bed 9 to this storm (Table S3).

From our analysis of the different storms that leave coarse horizons in CAOS7, we conclude that the CAOS blue hole captures predominately hurricanes that track to the south of the Caicos Islands. The reefs and island land masses to the north of the Caicos platform interior protect the platform from waves and storm surge associated with the front-end of northward passing hurricanes. It is unlikely that the intense hurricanes that passed to the north of the Caicos Islands (i.e., Hurricane Donna, 1960; 1933 Category 5 hurricane) generated an event bed in the CAOS blue hole. We show that our CAOS7 record is sensitive to all Category 1 and above storms that pass within 50 km to the south of Middle Caicos as well as higher intensity storms (e.g., Hurricane Irma in 2017) that track further away from the site (>50 km away and skirt south of the platform interior) (Figs. 8 and 10).

4.3. Caribbean site comparison

In the last few years, sediment cores from blue holes on Abaco Island (van Hengstum et al., 2014; Winkler et al., 2020), South Andros Island (Wallace et al., 2019), and Long Island (Wallace et al., 2021) have reconstructed hurricane activity in The Bahamas. All these reconstructions are near-annually resolved, record event deposits from proximal passing hurricanes of varying intensities (Long Island/Abaco Island: ≥Category 2; South Andros: ≥Category 3) and extend back 700 years or more. Middle Caicos Island lies to the southeast of all of these sites, approximately 380 km from Long Island and greater than 600 km away from South Andros and Abaco (Fig. 7). When comparing all The Bahamas records to our Middle Caicos cores (Fig. 11), we find varying levels of coherency among these records over the past two millennia.

During the first millennium of the record, we find fairly similar patterns of activity to the South Andros record (Wallace et al., 2019). South Andros was struck by more hurricanes from 640 to 815 CE and 920 to 1035 CE. Similarly, Middle Caicos captures 6 events from 660 to 725 CE, and 10 events from 960 to 1100 CE. Neither the Long Island or the Abaco Island records extend back far enough in time to capture activity in the 7th or 8th centuries (Fig. 11). The similarities with the South Andros record fade during the first half of the last millennium (1100–1500 CE). Middle Caicos

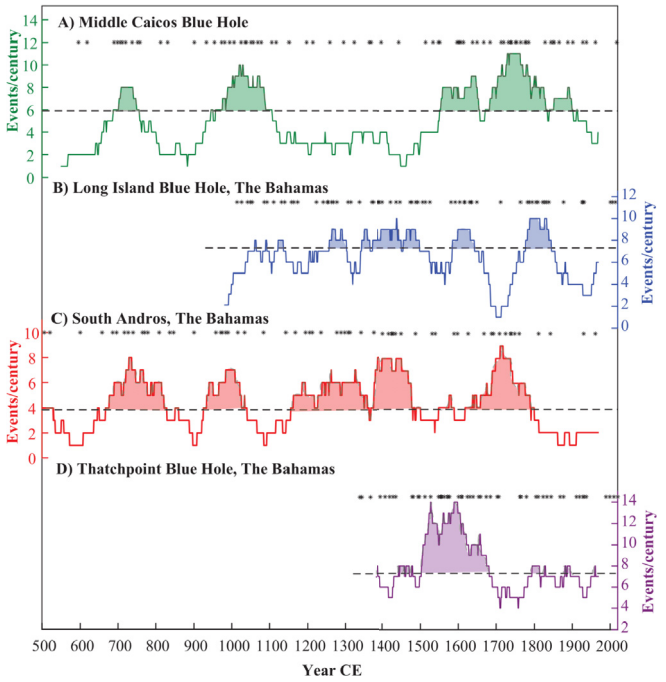

Fig. 11. 100-year moving window event frequency for Bahamas blue hole reconstructions: (A) Middle Caicos Blue Hole with 3 active intervals highlighted in green (B) Long Island Blue Hole (Wallace et al., 2021) with 4 active intervals highlighted in blue, (C) South Andros stacked record (Wallace et al., 2019; Winkler et al., 2020) with 4 active intervals highlighted in red, and (D) Thatchpoint Blue Hole (Winkler et al., 2020) with one active interval highlighted in purple. The timing of events in the records is denoted by the black stars above each panel. The black dashed lines on each panel indicate the upper 90% threshold for active periods at each site.

observed very few storms strikes over this interval while Long Island and South Andros showed intervals of elevated activity from 1200 to 1300 CE and 1350 to 1500 CE at Long Island and 1150 to 1450 CE at South Andros (Fig. 11).

Starting in the 16th century, reconstructed hurricane activity from Long Island and Middle Caicos is well aligned. Long Island observed increased event deposits from 1600 to 1655 CE with a drop off in activity in the late 17th century (much like that seen on Middle Caicos). This quiet interval is followed by another interval of increased activity on Long Island from 1775 to 1840 CE, still matching Middle Caicos (Fig. 11). However, none of the other Bahamian reconstructions detect increased activity over the last active period on Middle Caicos (1850–1910 CE).

The varying coherency between our Middle Caicos record and other records from the northern Bahamas likely reflects the different populations of the storms that impact each site. For example, of the 27 storms that passed within 100 km of Middle Caicos since 1851 CE, only six passed close enough (75 km radius) to Long Island blue hole (Wallace et al., 2021) to leave a coarse deposit (Fig. 7). The stochastic nature of TCs (Wallace et al., 2020) plays a significant role in determining where a given storm tracks and at what exact intensity it makes landfall. With all of these Bahamian sites capturing only proximal passing storms (100 km radii or less), hurricanes can pass through The Bahamas without impacting a single one of the current paleohurricane study sites. This is further complicated by recent work from Long Island in The Bahamas (Wallace et al., 2021) and northwest Florida (Lin et al., 2014) suggesting that storm properties other than intensity play a role in determining if a storm will generate enough surge and wave action to leave a coarse deposit. Both studies highlight that a storm's orientation and radius of maximum winds impact whether it will leave deposits. In addition, local site characteristics (e.g., coastline geometry, sediment sources, subtidal vs. intertidal geographic positioning) can also play a role in whether a blue hole site captures and preserves a coarse-grained event layer in the stratigraphic record (Wallace et al., 2019, 2021, 2021; van Hengstum et al., 2020).

Given that each site is capturing slightly different populations of storms, we can begin to understand how Bahamian hurricane activity has changed at a broader spatial scale over the past millennium by acquiring a higher density of individual sites in the Bahamas, and then compiling them together into a single reconstruction. This composite reconstruction will more coherently reflect the broad population of storms that have traveled in this region and remove some of the site-specific and random variability.

4.4. Basin-wide comparison

Using the same methods detailed in Wallace et al. (2021) and reviewed in Supplemental Section S2, we create a new compilation of paleohurricane records from the Bahama Archipelago including our Middle Caicos reconstruction. Our new compilation of blue hole paleohurricane reconstructions stretches from 500 to 2019 CE (Fig. 12) and encompasses both the northern and southern Bahama Archipelago including sites on South Andros (Wallace et al., 2019), Long Island (Wallace et al., 2021), Abaco Island (Winkler et al., 2020), and Middle Caicos. Each single paleohurricane proxy samples only certain storms passing near to each island and provides a record of local hurricane climate which may be dominated by stochasticity (Wallace et al., 2020). Using a large set of downscaled storms run using the National Center for Environmental Prediction (NCEP) Reanalysis climate (1949–2015 CE), we found that compiling the storms captured by all four of these sites into a single record explains approximately 80% of the variance in the frequency of all the synthetic storms passing through the Bahama Archipelago (Fig. S5). Therefore, even though this compilation only captures approximately 58% of the storms passing through the Bahama Archipelago (Supplemental Section S3), it represents the variance in storm frequency in the Bahama Archipelago well. This suggests that we can use compilations of individual event-based paleohurricane records (i.e., Bahamas blue hole sites) with different limited sensitivities (i.e., only intense hurricanes) to approximate the underlying variations in regional hurricane frequency (tropical storms through Category 5 hurricanes).

Our new compilation shows increased hurricane activity from 650 to 800 CE, 930 to 1040 CE, and 1400 to 1800 CE. After 1800 CE, we see a decrease in the number of storms observed in the Bahama Archipelago. We compare this new regional compilation from The Bahamas to two other similarly resolved compilations of paleohurricane records from New England and the Gulf Coast of Florida (Fig. 12). These compilations were originally presented in Wallace et al. (2021); we summarize the methodology and components for both compilations in Supplemental Section S2. We generate both a High Threshold (HT- Category 3 and above) and Low Threshold (LT- Category 1 and above) estimate for the Gulf Coast of Florida. Each compilation likely captures a very different set of storms over the past millennium, but by comparing these spatially disparate compilations, we offer insights into the shifting predominance of regional storm activity in the North Atlantic.

All three regional compilations (New England, Gulf Coast of Florida, Bahama Archipelago) document multi-decadal phases of elevated hurricane activity over past millennium, both synchronous and asynchronous (Fig. 12). Long-term regional hurricane activity is likely modulated by broad-scale patterns in SSTs and vertical wind shear in the North Atlantic. In the past 50 years, natural decadal climate variability in the Atlantic (i.e., the Atlantic Multidecadal Variability (AMV)) systematically created different environmental conditions along the U.S. East Coast and Gulf Coast.

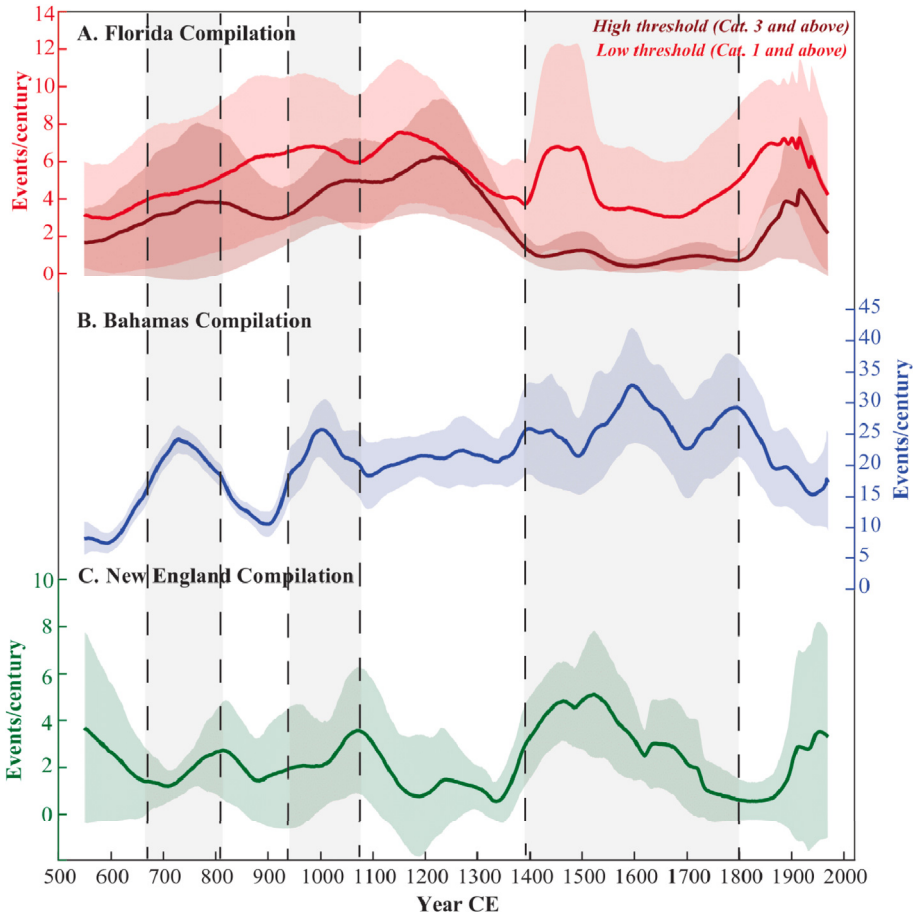

Fig. 12. Compilations of paleohurricane records from (A) northwest Florida (red) including records from Mullet Pond (Lane et al., 2011), Spring Creek Pond (Brandon et al., 2013), Shotgun Pond and Basin Bayou (Rodysill et al., 2020) (B) The Bahama Archipelago (blue) including all the records shown in Fig. 11 and (C) New England (green) including records from Salt Pond, MA (Donnelly et al., 2015) and Mattapoisett Marsh (Boldt et al., 2010; Castagno et al., 2021). The shaded confidence intervals are calculated from the spread in each of the contributing records. All three compilations shown were smoothed with a 100-year moving window. The original compilations (without the filter) are shown in Figs. S6–S7. For the Florida compilation, we include a High Threshold (dark red - Category 3 and above) and Low Threshold (red - Category 1 and above) estimate. Grey boxes highlight local maxima in storms identified in the Bahama Archipelago Compilation.

Positive phases of the AMV set up a protective barrier of enhanced vertical wind shear along U.S. East Coast preventing many storms from intensifying along the U.S. East Coast (Kossin, 2017). Anthropogenic warming is expected to induce the opposite pattern with unfavorable vertical wind shear patterns in the Gulf of Mexico and Caribbean Sea but not the U.S. East Coast (Ting et al., 2019). This anthropogenic vertical wind shear pattern is largely thought to be driven by predicted Hadley cell expansion (Lu et al., 2007; Kang and Lu, 2012) and a subsequent northward shift in the mid-latitude jet (Barnes and Polvani, 2013).

In addition, changes in storm track populations likely also contribute to regional patterns of hurricane activity in the North Atlantic. Changes in the North Atlantic Subtropical High (NASH), a semi-permanent high pressure system that resides over the North Atlantic in the Northern hemisphere summer, affect the steering currents that determine Atlantic hurricane tracks (Ortegren and Maxwell, 2014). In particular, a weaker and/or northeastward displaced NASH steers hurricane tracks along the U.S. East Coast around the western edge of the high. A southwestward displaced NASH, on the other hand, maintains easterly currents and pushes more storms into the Gulf of Mexico (Elsner, 2003; Kossin et al., 2010; McCloskey et al., 2013; Ortegren and Maxwell, 2014).

In the context of our records, from 600 to 800 CE, we observe fewer storms in New England accompanied by more frequent storm strikes in the Bahama Archipelago and in northwest Florida (Fig. 12). Perhaps during this time span, there were more storms forming and traveling in the tropical Atlantic, but there were unfavorable vertical wind shear patterns along the U.S. East coastline and/or a southwestward displaced NASH generating easterly steering currents. In either case, storms forming in the tropical Atlantic would tend toward a straighter westward-moving storm population tracking through the Bahama Archipelago and Gulf of Mexico.

During the Medieval Climate Anomaly (MCA) from 950 to 1250 CE (Mann et al., 2009b), all three regions (New England, Gulf Coast of Florida, Bahama Archipelago) document elevated storm activity at some point. In the Bahama Archipelago and New England, this elevated activity only occurs in the early MCA from 950 to 1050 CE. The Gulf Coast of Florida remains active throughout the entire MCA (Fig. 12). These three spatially disparate compilations support previous statistical modeling work suggesting that the early MCA was a time period with basin-wide increased storm activity (Mann et al., 2009a). Warmer sea surface temperatures (SSTs) in the North Atlantic Main Development Region (Mann, 2002) and La-Niña-like conditions in the eastern Pacific from 900 to 1100 CE likely contributed to more storms forming in the North Atlantic basin. Simultaneously, a persistently positive phase of the AMV during the MCA (Wang et al., 2017) could have contributed to favorable ocean and atmospheric states for hurricane intensification in the western North Atlantic, particularly the Gulf of Mexico. Meanwhile, the

decline in storm activity in the Bahamas and New England during the late half of the MCA could be a result of development of enhanced shear along the U.S. East Coast/Bahamas related to the positive AMV phase (Kossin, 2017; Ting et al., 2019).

Following this MCA peak in storm activity, both the Bahama Archipelago and New England reconstructions indicate a lower storm frequency during the next few centuries (1200 to 1400 CE) (Fig. 10). Within this quiet interval, The Bahama Archipelago compilation indicates a smaller peak in activity in the 13th century (Fig. 12). The 13th century was characterized by abundant volcanic eruptions, including the largest eruption on record, the 1257 Samalas eruption in Indonesia (Gao et al., 2008; Sigl et al., 2014). The blue hole paleohurricane reconstruction from South Andros Island (Wallace et al., 2019) indicates an unusual gap in storm strikes over this same time interval (1204–1273 CE). Wallace et al. (2019) suggested that this gap in activity was connected to short-term reductions in TC intensity in the North Atlantic related to oceanic cooling in the aftermath of the 13th century volcanic eruptions. However, more recent records from Middle Caicos Island and Long Island (Wallace et al., 2021) document more storm strikes during the 13th century resulting in the subdued peak in activity observed in our compilation (Figs. S6–S7). This new compilation suggests that the gap in activity documented in the South Andros cores was more likely a randomly driven local signal in hurricane activity, and not a climate driven regional signal. More work is needed to establish a robust relationship between past millennium volcanic eruptions and TC distributions in the North Atlantic.

During Little Ice Age (LIA: 1400–1700; Mann et al., 2009b), we observe elevated hurricane activity in the Bahama Archipelago and along U.S. East Coast while the Florida Gulf Coast is relatively quiet (Fig. 12). At the onset of the LIA, we observe a short-lived peak in activity from ~1420 to 1510 CE in the Florida LT compilation, suggesting that the Gulf Coast of Florida was hit by many low intensity events (Category 1–2) at the same time New England and The Bahamas started experiencing increased storm strikes. AMV reconstructions for past millennium (Mann et al., 2009b; Wang et al., 2017) suggest that there was a persistently negative phase during the LIA, particularly at its onset (15th century). Perhaps high vertical wind shear in the Gulf of Mexico resulting from a negative AMV prevented storms from intensifying before they made landfall along the Gulf Coast of Florida. In addition, this shift in the 1400's towards more storms striking along U.S. East Coast and Bahamas and fewer storms in the Gulf could also signify a transition towards more recurving storm tracks perhaps tied to northward shift in the mid-latitude jet and NASH. We currently lack the paleo reconstructions for either the NASH or North Atlantic mid-latitude jet that are required to test these hypotheses.

Overall, The Bahama Archipelago experienced a substantial reduction in storm activity during the past 200 years compared to any other time over the last millennium (1000 to 2020 CE). The Gulf Coast of Florida, on the other hand, shows increased storm strikes from 1780 to 1950 CE (Fig. 12A- LT Compilation). In particular, records from Apalachee Bay (Lane et al., 2011; Brandon et al., 2013; Rodysill et al., 2020) in Florida capture eight low intensity storm strikes across this interval (Figs. S6–S7). The New England compilation remains inactive for much of the 18th and 19th centuries (Fig. 12). However, this inactivity may be a result of the sensitivity of the New England sites (Donnelly et al., 2015). Both the Salt Pond (Donnelly et al., 2015) and Mattapoisett Marsh (Boldt et al., 2010; Castagno et al., 2021) reconstructions capture Category 2 and above hurricanes. Documentary records suggest many lower intensity storms (<Category 2) impacted the U.S. Northeast Coast during the 1800s (Ludlum, 1997; Boose et al., 2001). Starting around 1900 CE, we begin to observe an increase in storm activity in our New England compilation (Fig. 12). With anthropogenic warming, we should expect this pattern to continue. With predicted future expansion of the Hadley cell (Lu et al., 2007; Kang and Lu, 2012) and warmer SST's expanding into the subtropical North Atlantic (Ting et al., 2015), storms are predicted to make landfall more often along the U.S. East Coast (Ting et al., 2019).

5. Conclusions

Here, we reconstruct hurricane strikes on Middle Caicos Island over the past 1520 years from blue hole sediment cores. We find large coarse-grained deposits that can be tracked across a transect of three cores each approximately 100 m apart. We attribute the top nine coarse event beds to historical hurricanes passing within 100 km of the island. We find that the orientation of passing storms with respect to the site is more important than storm intensity for inducing coarse-grained sediment transport on the Caicos platform interior. Indeed, low intensity storms, like Hurricane Kate in 1985, that pass to the south of the island leave deposits in the Middle Caicos blue hole while other high intensity storms that passed on the northern side of Turks & Caicos, like Hurricane Donna in 1960, do not. This finding corroborates previous work studying storm deposits on Long Island, The Bahamas (Wallace et al., 2021) which indicates storm surge can depend greatly on both coastal geometry and storm properties (i.e., size, speed and angle of approach). It also highlights the need for additional detailed hydrodynamic modeling studies on Caribbean islands (e.g., Sahoo et al., 2019) investigating how storms of different properties and tracks influence surge and wave generation.

Taken as a whole, our record from Middle Caicos indicates elevated storm strikes in three multi-decadal periods over the past 1520 years from 690 to 760 CE, 960 to 1100 CE, and 1550 to 1900 CE. Like previous work (Wallace et al., 2021), this record matches well with some neighboring records from The Bahamas and poorly with others. Ultimately, each paleohurricane site is sampling some small subset of storms passing through The Bahamas. We stress the need for compilations of large numbers of paleohurricane records from a region to capture regional changes in hurricane climate.

We update regional compilations of paleohurricane activity for the past millennium in New England, The Bahamas, and the Gulf Coast of Florida. These records indicate synchronous and diverging periods of elevated hurricane activity. Synchronous active periods occurred during the Medieval Climate Anomaly from 900 to 1100 CE and during the 15th century. We argue these periods correspond to basin-wide elevated hurricane activity characterized by warmer sea surface temperatures in the Atlantic. Diverging active periods occur from 600 to 800 CE and 1500 to 1800 CE and are characterized by more activity in New England when the Gulf Coast is quiet. We argue that regional scale patterns in vertical wind shear and/or shifting storm populations contributed to these diverging active periods. Reconstructions of the North Atlantic Subtropical High and mid-latitude jet for the past two millennium are needed to discern drivers of these centennial-scale patterns in hurricane landfalls.

Data availability

The data are available on the National Climatic Data Center (https://www.ncdc.noaa.gov/paleo/study/33652) and WHOI Coastal Systems Group (https://web.whoi.edu/coastal-group/data) websites.

Declaration of competing interest

The authors declare that they have no known competing financial interests or personal relationships that could have appeared to influence the work reported in this paper.

Acknowledgements

This work was funded by the National Science Foundation Graduate Research Fellowship (to E.J.W.), the Dalio Explore Foundation, and National Science Foundation grants OCE-1356708 (to J.P.D. and P.J.vH.), PREEVENTS-1854980 (to J.P.D. and P.J.vH.), and P2C2-1903616 (to J.P.D. and P.J.vH.). Additional technical support was provided by Stephanie Madsen, Rose Palermo, Kelly McKeon, Shawna Little, Annie Tamalvage, Dan Litchmore, and Lizzy Sorrano. We thank Kerry Emanuel for providing us with the NCEP synthetic storm dataset. We thank two anonymous reviewers for their constructive comments that helped to improve this paper.

Credit author statement

E. J. Wallace: Conceptualization, Methodology, Software, Validation, Formal analysis, Investigation, Data curation, Writing – original draft, Writing-Reviewing & Editing, Supervision, Project administration, J. P. Donnelly: Conceptualization, Methodology, Resources, Writing-Reviewing & Editing, Supervision, Project administration, Funding acquisition, P. J. van Hengstum: Conceptualization, Methodology, Writing-Reviewing & Editing, Project administration, Funding acquisition, T. S. Winkler: Methodology, Investigation, Writing-Reviewing & Editing, C. Dizon: Investigation, Writing-Reviewing & Editing, Funding acquisition, A. LaBella: Investigation, Writing-Reviewing & Editing, I. Lopez: Investigation, Writing-Reviewing & Editing. N. E. d'Entremont: Investigation, Writing-Reviewing & Editing, Supervision, Project administration. R. M. Sullivan: Investigation, Writing-Reviewing & Editing. J. D. Woodruff: Investigation, Writing-Reviewing & Editing. A. D. Hawkes: Investigation, Writing-Reviewing & Editing. C. Maio: Investigation, Writing-Reviewing & Editing.

Appendix A. Supplementary data

Supplementary data to this article can be found online at https://doi.org/10.1016/j.quascirev.2021.107126.

References

Anselmetti, F.S., Eberli, G.P., 1993. Controls on sonic velocity in carbonates. Pure and Applied Geophysics PAGEOPH 141, 287–323. https://doi.org/10.1007/BF00998333.

Barnes, E., Polvani, L., 2013. Response of the midlatitude jets, and of their variability, to increased greenhouse gases in the CMIP5 models. J. Clim. 26, 7117–7135. https://doi.org/10.1175/JCLI-D-12-00536.1.

Blaauw, M., Christen, J.A., 2011. Flexible paleoclimate age-depth models using an autoregressive gamma process. Bayesian Analysis 6, 457–474. https://doi.org/10.1214/11-BA618.

Boldt, K.V., Lane, P., Woodruff, J.D., Donnelly, J.P., 2010. Calibrating a sedimentary record of overwash from Southeastern New England using modeled historic hurricane surges. Mar. Geol. 275, 127–139. https://doi.org/10.1016/j.margeo.2010.05.002.

Boose, E.R., Chamberlin, K.E., Foster, D.R., 2001. Landscape and regional impacts of hurricanes in New England. Ecol. Monogr. 71, 27–48. https://doi.org/10.1890/0012-9615(2001)071[0027:LARIOH]2.0.CO;2.

Bramante, J.F., Ford, M.R., Kench, P.S., Ashton, A.D., Toomey, M.R., Sullivan, R.M., Karnauskas, K.B., Ummenhofer, C.C., Donnelly, J.P., 2020. Increased typhoon activity in the Pacific deep tropics driven by Little Ice Age circulation changes. Nat. Geosci. 13, 806–811. https://doi.org/10.1038/s41561-020-00656-2.

Brandon, C.M., Woodruff, J.D., Lane, D.P., Donnelly, J.P., 2013. Tropical cyclone wind speed constraints from resultant storm surge deposition: a 2500 year reconstruction of hurricane activity from St. Marks, FL. G-cubed 14, 2993–3008. https://doi.org/10.1002/ggge.20217.

Bregy, J.C., Wallace, D.J., Minzoni, R.T., Cruz, V.J., 2018. 2500-year paleotempestological record of intense storms for the northern Gulf of Mexico, United States. Mar. Geol. https://doi.org/10.1016/j.margeo.2017.09.009.

Camargo, S.J., Emanuel, K., Sobel, A.H., 2007. Use of a genesis potential index to diagnose ENSO effects on tropical cyclone genesis. J. Clim. 20, 4819–4834. https://doi.org/10.1175/JCLI4282.1.

Cangialosi, J.P., Latto, A.S., Berg, R., 2018. Hurricane Irma (AL112017).

Carew, J.L., Mylroie, J.E., 1995. Quaternary tectonic stability of the Bahamian archipelago: evidence from fossil coral reefs and flank margin caves. Quat. Sci. Rev. 14, 145–153. https://doi.org/10.1016/0277-3791(94)00108-N.

Castagno, K.A., Donnelly, J.P., Woodruff, J.D., 2021. Grain-size analysis of hurricane-induced event beds in a new England salt Marsh, Massachusetts, USA. J. Coast Res. 37, 326–335. https://doi.org/10.2112/JCOASTRES-D-19-00159.1.

Chu, P., 2004. ENSO and tropical cyclone activity. In: Murnane, R.J., Liu, K. (Eds.), Hurricanes and Typhoons: Past, Present, and Future. Columbia University Press, New York, pp. 297–332.

Clement, A., Bellomo, K., Murphy, L.N., Cane, M.A., Mauritsen, T., Stevens, B., 2015. The Atlantic Multidecadal Oscillation without a role for ocean circulation. Science 350, 320–324. https://doi.org/10.1126/science.aab3980.

Deines, P., 1980. The isotopic composition of reduced organic carbon. In: Fritz, P., Fontes, J.C. (Eds.), Handbook of Environmental Isotope Geochemistry, vol. 1. Elsevier, New York, pp. 329–406.

Denommee, K.C., Bentley, S.J., Droxler, A.W., 2014. Climatic controls on hurricane patterns: a 1200-y near-annual record from Lighthouse Reef. Belize: Sci. Rep. 4. https://doi.org/10.1038/srep03876.

Dinan, T., Hanon, T., Sperl, J., 2016. Potential Increases in Hurricane Damage in the united states: Implications for the Federal Budget.

Donnelly, J.P., Hawkes, A.D., Lane, P., Macdonald, D., Shuman, B.N., Toomey, M.R., Van Hengstum, P.J., Woodruff, J.D., 2015. Climate forcing of unprecedented intense-hurricane activity in the last 2000 years. Earth's Future 3, 49–65. https://doi.org/10.1002/2014EF000274.

Dravis, J.J., Wanless, H.R., 2017. Impact of strong easterly trade winds on carbonate petroleum exploration - relationships developed from Caicos Platform. southeastern Bahamas: Mar. Petrol. Geol. 85, 272–300. https://doi.org/10.1016/j.marpetgeo.2017.04.010.

Duarte, C.M., et al., 2018. Stable isotope (δ13C, δ15N, δ18O, δD) composition and nutrient concentration of red sea primary producers. Frontiers in Marine Science 5, 1–12. https://doi.org/10.3389/fmars.2018.00298.

Dunn, G.E., 1961. The Hurricane Season of 1960: Monthly Weather Review, pp. 99–108.

Elsner, J.B., 2003. Tracking hurricanes. Bull. Am. Meteorol. Soc. 84, 353–356. https://doi.org/10.1175/BAMS-84-3-353.

Elsner, J.B., Kocher, B., 2000. Global tropical cyclone activity: a link to the north atlantic oscillation. J. Geophys. Res. 27, 129–132. https://doi.org/10.1029/1999GL010893.

Emanuel, K., 1987. The dependence of hurricane intensity on climate. Nature 326, 483–485.

Emanuel, K., 1989. The finite-amplitude nature of tropical cyclogenesis. J. Atmos. Sci. 46, 3431–3456.

Emanuel, K., 1988. The maximum intensity of hurricanes. J. Atmos. Sci. 45, 1143–1155.

Emanuel, K., 2003. Tropical Cyclones: Annu. Rev. Earth Planet Sci. 31, 75–104. https://doi.org/10.1146/annurev.earth.31.100901.141259.

Emanuel, Kerry, Ravela, Sai, Vivant, Emmanuel, Risi, Camille, 2006. A statistical deterministic approach to hurricane risk assessment. Bull. Am. Meteorol. Soc. 87 (3), 299–314. https://doi.org/10.1175/BAMS-87-3-299.

Emanuel, Kerry, Sundararajan, Ragoth, Williams, John, 2008. Hurricanes and global warming: Results from downscaling IPCC AR4 simulations. Bull. Am. Meteorol. Soc. 89 (3), 347–367. https://doi.org/10.1175/BAMS-89-3-347.

Evan, A.T., 2012. Atlantic hurricane activity following two major volcanic eruptions. J. Geophys. Res.: Atmosphere 117, n/a. https://doi.org/10.1029/2011JD016716 n/a.

Gao, C., Robock, A., Ammann, C., 2008. Volcanic forcing of climate over the past 1500 years: an improved ice core-based index for climate models. Journal of Geophysical Research Atmospheres 113, 1–15. https://doi.org/10.1029/2008JD010239.

Gischler, E., Anselmetti, F.S., Shinn, E.A., 2013. Seismic stratigraphy of the blue hole (Lighthouse reef, Belize), a late Holocene climate and storm archive. Mar. Geol. 344, 155–162. https://doi.org/10.1016/j.margeo.2013.07.013.

Gischler, E., Shinn, E.A., Oschmann, W., Fiebig, J., Buster, N.A., 2008. A 1500-year Holocene caribbean climate archive from the blue hole, Lighthouse reef, Belize. J. Coast Res. 246, 1495–1505. https://doi.org/10.2112/07-0891.1.

Goldenberg, S.B., Landsea, C.W., Mestas-Nuñez, A.M., Gray, W.M., 2001. The recent increase in atlantic hurricane activity: causes and implications. Science 293, 474–479. https://doi.org/10.1126/science.1060040.

Goldenberg, S.B., Shapiro, L.J., 1996. Physical mechanisms for the association of El Niño and west African rainfall with Atlantic major hurricane activity. J. Clim. 9, 1169–1187. https://doi.org/10.1175/1520-0442(1996)009<1169:PMFTAO>2.0.CO;2.

Gray, W.M., 1984. Atlantic seasonal hurricane frequency. Part I: El Niño and 30 mb quasi-biennial oscillation influences. Mon. Weather Rev. 112, 1649–1668. https://doi.org/10.1175/1520-0493(1984)112<1649:ASHFPI>2.0.CO;2.

Gray, W.M., 1998. The Formation of Tropical Cyclones: Meteorology and Atmospheric Physics, vol. 67, pp. 37–69. https://doi.org/10.1007/BF01277501.

Hall, T., Hereid, K., 2015. The Frequency and Duration of U.S. Hurricane Droughts. Geophysical Research Letters, pp. 3482–3485. https://doi.org/10.1002/2015GL063652.

van Hengstum, P.J., Donnelly, J.P., Fall, P.L., Toomey, M.R., Albury, N.A., Kakuk, B., 2016. The intertropical convergence zone modulates intense hurricane strikes on the western North Atlantic margin. Sci. Rep. 6, 21728. https://doi.org/10.1038/srep21728.

van Hengstum, P.J., Donnelly, J.P., Toomey, M.R., Albury, N.A., Lane, P., Kakuk, B., 2014. Heightened hurricane activity on the little Bahama bank from 1350 to

1650 AD. Continent. Shelf Res. 86, 103–115. https://doi.org/10.1016/j.csr.2013.04.032.
van Hengstum, P.J., Winkler, T.S., Tamalavage, A.E., Sullivan, R.M., Little, S.N., Macdonald, D., Donnelly, J.P., Albury, N.A., 2020. Holocene sedimentation in a blue hole surrounded by carbonate tidal flats in the Bahamas: autogenic versus allogenic processes. Mar. Geol. 419. https://doi.org/10.1016/j.margeo.2019.106051.
Jamison-Todd, S., 2019. Hurricane Irma Deposits on Modern Carnonate Platform. University of Colorado at Boulder, pp. 1–35.
Kaczmarek, S.E., Hasiuk, F., 2008. Mapping surficial sediment distributions on Caicos Platform: a quantitative approach integrating statistical analysis of Landsat spectral data and field observations. In: Morgan, W.A., Harris, P.M. (Eds.), Developing Models and Analogs for Isolated Carbonate Platforms—Holocene and Pleistocene Carbonates of Caicos Platform. British West Indies, Society for Sedimentary Geology, pp. 57–72. https://doi.org/10.2110/pec.08.22.0057.
Kang, S.M., Lu, J., 2012. Expansion of the Hadley cell under global warming: winter versus summer. J. Clim. 25, 8387–8393. https://doi.org/10.1175/JCLI-D-12-00323.1.
Knapp, K., Kruk, M.C., Levinson, D.H., Diamond, H.J., Neumann, C.J., 2010. The international best track archive for climate stewardship (IBTrACS). Bull. Am. Meteorol. Soc. 91, 363–376. https://doi.org/10.1175/2009BAMS2755.1.
Knutson, T., et al., 2020. Tropical Cyclones and Climate Change Assessment Part II: Projected Response to Anthropogenic Warming. Bulletin of the American Meteorological Society, pp. 303–322. https://doi.org/10.1175/BAMS-D-18-0194.1.
Kohn, M.J., 2010. Carbon isotope compositions of terrestrial C3 plants as indicators of (paleo) ecology and (paleo) climate. Proc. Natl. Acad. Sci. Unit. States Am. 107, 19691–19695. https://doi.org/10.1073/pnas.1004933107.
Korty, R.L., Camargo, S.J., Galewsky, J., 2012. Variations in tropical cyclone genesis factors in simulations of the Holocene epoch. J. Clim. 25, 8196–8211. https://doi.org/10.1175/JCLI-D-12-00033.1.
Kossin, J.P., 2017. Hurricane intensification along United States coast suppressed during active hurricane periods. Nature 541, 390–393. https://doi.org/10.1038/nature20783.
Kossin, J.P., Camargo, S.J., Sitkowski, M., 2010. Climate modulation of North Atlantic hurricane tracks. J. Clim. 23, 3057–3076. https://doi.org/10.1175/2010JCLI3497.1.
Landsea, W.C., Anderson, C., Charles, N., Clark, G., Dunion, J., Partagas, J., Hungerford, P., Neumann, C., Zimmer, M., 2004. The Atlantic Hurricane Database Reanalysis Project: Documentation for 1851-1910 Alterations and Additions to the HURDAT Database, pp. 178–221. http://www.aoml.noaa.gov/hrd/Landsea/rpibook-final04.pdf.
Landsea, C.W., Franklin, J.L., 2013. Atlantic hurricane database uncertainty and presentation of a new database format. Mon. Weather Rev. 141, 3576–3592. https://doi.org/10.1175/MWR-D-12-00254.1.
Landsea, C.W., Vecchi, G.A., Bengtsson, L., Knutson, T.R., 2010. Impact of duration thresholds on Atlantic tropical cyclone counts. J. Clim. 23, 2508–2519. https://doi.org/10.1175/2009JCLI3034.1.
Lane, P., Donnelly, J.P., Woodruff, J.D., Hawkes, A.D., 2011. A decadally-resolved paleohurricane record archived in the late Holocene sediments of a Florida sinkhole. Mar. Geol. 287, 14–30. https://doi.org/10.1016/j.margeo.2011.07.001.
Lin, N., Lane, P., Emanuel, K.A., Sullivan, R.M., Donnelly, J.P., 2014. Heightened hurricane surge risk in northwest Florida revealed from climatological-hydrodynamic modeling and paleorecord reconstruction. J. Geophys. Res.: Atmosphere 119, 1–18. https://doi.org/10.1002/2014JD021584.
Lu, J., Vecchi, G.A., Reichler, T., 2007. Expansion of the Hadley cell under global warming. Geophys. Res. Lett. 34, 2–6. https://doi.org/10.1029/2006GL028443.
Ludlum, D.M., 1997. Early American Hurricanes 1492-1870: Boston. American Meterological Society, pp. 1910–1997.
Mallinson, D.J., Smith, C.W., Mahan, S., Culver, S.J., McDowell, K., 2011. Barrier island response to late Holocene climate events. North Carolina, USA: Quat. Res. 76, 46–57. https://doi.org/10.1016/j.yqres.2011.05.001.
Mann, M., 2002. Medieval Climatic Optimum: Encyclopedia of Global Environmental Change, vol. 1, pp. 514–516. http://holocene.meteo.psu.edu/shared/articles/medclimopt.pdf%5Cnhttp://www.meteo.psu.edu/holocene/public_html/Mann/articles/articles/medclimopt.pdf.
Mann, M.E., Woodruff, J.D., Donnelly, J.P., Zhang, Z., 2009a. Atlantic hurricanes and climate over the past 1,500 years. Nature 460, 880–883. https://doi.org/10.1038/nature08219.
Mann, M.E., Zhang, Z., Rutherford, S., Bradley, R.S., Hughes, M.K., Shindell, D., Ammann, C., Faluvegi, G., Ni, F., 2009b. Global signatures and dynamical origins of the little ice age and medieval climate anomaly. Science 326, 1256–1260. https://doi.org/10.1126/science.1177303.
McCloskey, T., Bianchette, T., Liu, K., 2013. Track patterns of landfalling and coastal tropical cyclones in the Atlantic basin, their relationship with the north atlantic oscillation (NAO), and the potential effect of global warming. American Journal of Climate 2, 12–22. https://doi.org/10.4236/ajcc.2013.23A002.
Merrill, R.T., 1987. Environmental influences on hurricane intensification. J. Atmos. Sci. 45, 1678–1687.
National geophysical data center/world data Service NCEI/WDS global Historical Tsunami Database:, doi:10.7289/V5PN93H7.
Neely, W., 2014. The Great Okeechobee Hurricane of 1928: Bloomington. iUniverse LLC.
Neely, W., 2006. The major hurricanes to affect the Bahamas: bloomington. Author 1–258.
Ortegren, J.T., Maxwell, J.T., 2014. Spatiotemporal patterns of drought/tropical cyclone Co-occurrence in the southeastern USA: linkages to north atlantic climate variability. Geography Compass 8, 540–559.
Pasch, R.J., Penny, A.B., Berg, R., 2019. Hurricane Maria (AL152017).
Pausata, F.S.R., Camargo, S.J., 2019. Tropical Cyclone Activity Affected by Volcanically Induced ITCZ Shifts, vol. 116. https://doi.org/10.1073/pnas.1900777116.
Podlaha, Adam, Bowen, Steve, Daneshvaran, Siamak, Lörinc, Michal, Bhattacharya, Anwesha, 2018. Hurricane Irma event recap report. Aon Benfield.
Reimer, P.J., et al., 2020. The IntCal20 northern hemisphere radiocarbon age calibration curve (0-55 cal kBP). Radiocarbon 62, 725–757. https://doi.org/10.1017/RDC.2020.41.
Rios-Berrios, R., Torn, R.D., 2017. Climatological analysis of tropical cyclone intensity changes under moderate vertical wind shear. Mon. Weather Rev. 145, 1717–1738. https://doi.org/10.1175/MWR-D-16-0350.1.
Rodysill, J., et al., 2020. Historically unprecedented Northern Gulf of Mexico hurricane activity from 650 to 1250 CE. Sci. Rep. 10, 1–17. https://doi.org/10.1038/s41598-020-75874-0.
Sahoo, B., Jose, F., Bhaskaran, P.K., 2019. Hydrodynamic response of Bahamas archipelago to storm surge and hurricane generated waves – a case study for Hurricane Joaquin. Ocean Eng. 184, 227–238.
Schmitt, D., Gischler, E., Anselmetti, F.S., Vogel, H., 2020. Caribbean cyclone activity: an annually-resolved Common Era record. Sci. Rep. 10, 1–17. https://doi.org/10.1038/s41598-020-68633-8.
Schmitt, D., Gischler, E., Walkenfort, D., 2021. Holocene sediments of an inundated sinkhole: facies analysis of the "Great Blue Hole". Lighthouse Reef, Belize: Facies 67, 1–24. https://doi.org/10.1007/s10347-020-00615-8.
Shinn, E.A., Reich, C.D., Locker, S.D., Hine, A.C., 1996. A giant sediment trap in the Florida keys. J. Coast Res. 12, 953–959.
Sigl, M., et al., 2014. Insights from Antarctica on volcanic forcing during the common era. Nat. Clim. Change 4, 693–697. https://doi.org/10.1038/nclimate2293.
Ting, M., Camargo, S.J., Li, C., Kushnir, Y., 2015. Natural and forced North Atlantic hurricane potential intensity change in CMIP5 models*. J. Clim. 28, 3926–3942. https://doi.org/10.1175/JCLI-D-14-00520.1.
Ting, M., Kossin, J.P., Camargo, S.J., Li, C., 2019. Past and future hurricane intensity change along the. U. S. East Coast: Sci. Rep. 9, 1–8. https://doi.org/10.1038/s41598-019-44252-w.
Trower, E.J., et al., 2018. Active ooid growth by sediment transport in a high-energy shoal, Little Ambergris Cay, Turks and Caicos Islands. J. Sediment. Petrol. 88, 1132–1151. https://doi.org/10.2110/jsr.2018.59.
Trower, E.J., Lamb, M.P., Fischer, W.W., 2019. The Origin of Carbonate Mud. Geophysical Research Letters, pp. 2696–2703. https://doi.org/10.1029/2018GL081620.
Ulm, K., 1990. A simple method to calculate the confidence interval of a standardized mortality ratio (SMR). Am. J. Epidemiol. 131, 373–375. https://doi.org/10.1093/oxfordjournals.aje.a115507.
Vecchi, G.A., Knutson, T.R., 2011. Estimating annual numbers of Atlantic hurricanes missing from the HURDAT database (1878-1965) using ship track density. J. Clim. 24, 1736–1746. https://doi.org/10.1175/2010JCLI3810.1.
Vecchi, G.A., Knutson, T.R., 2008. On estimates of historical North Atlantic tropical cyclone activity. J. Clim. 21, 3580–3600. https://doi.org/10.1175/2008JCLI2178.1.
Villarini, G., Vecchi, G.A., Knutson, T.R., Smith, J.A., 2011. Is the recorded increase in short-duration North Atlantic tropical storms spurious? Journal of Geophysical Research Atmospheres 116, 1–11. https://doi.org/10.1029/2010JD015493.
Wallace, E.J., et al., 2021. 1050 Years of Hurricane Strikes on Long Island in the Bahamas: Paleoceanography and Paleoclimatology.
Wallace, E.J., Coats, S., Emanuel, K.A., Donnelly, J.P., 2020. Centennial-scale shifts in storm frequency captured in paleohurricane records from the Bahamas arise predominantly from random variability. Geophys. Res. Lett. https://doi.org/10.1029/2020GL091145.
Wallace, E.J., Donnelly, J.P., van Hengstum, P.J., Wiman, C., Sullivan, R.M., Winkler, T.S., D'Entrement, N.E., Toomey, M.R., Albury, N.A., 2019. Intense hurricane activity over the past 1500 years at South Andros island. The Bahamas: Paleoceanography and Paleoclimatology 34, 1761–1783. https://doi.org/10.1029/2019PA003665.
Wang, J., Yang, B., Ljungqvist, F.C., Luterbacher, J., Osborn, T.J., Briffa, K.R., Zorita, E., 2017. Internal and external forcing of multidecadal Atlantic climate variability over the past 1,200 years. Nat. Geosci. 10, 512–517. https://doi.org/10.1038/ngeo2962.
Wanless, H.R., Tedesco, L.P., Tyrrell, K.M., 1988a. Production of subtidal tubular and surficial tempestites by hurricane kate, Caicos platform, British west indies. J. Sediment. Petrol. 58, 739–750.
Wanless, H.R., Tyrrell, K.M., Tedesco, L.P., Dravis, J.J., 1988b. Tidal-flat sedimentation from hurricane kate, Caicos platform, British west indies. J. Sediment. Petrol. 58, 724–738.
Wefer, G., Killingley, J.S., 1986. Carbon isotopes in organic matter from a benthic alga Halimeda incrassata (Bermuda): effects of light intensity. Chem. Geol. 59, 321–326.
Winkler, T.S., Van Hengstum, P.J., Donnelly, J.P., Wallace, E.J., Sullivan, R.M., Macdonald, D., Albury, N.A., 2020. Revising evidence of hurricane strikes on Abaco Island (The Bahamas) over the last 680 years. Sci. Rep. 10. https://www.nature.com/articles/s41598-020-73132-x.